Check for updates

View Article Online
View Journal

RSC Sustainability

Accepted Manuscript

This article can be cited before page numbers have been issued, to do this please use: S. A. Thomas, J. Cherusseri, A. Kumar and D. N. Rajendran, *RSC Sustainability*, 2025, DOI: 10.1039/D5SU00525F.

This is an Accepted Manuscript, which has been through the Royal Society of Chemistry peer review process and has been accepted for publication.

Accepted Manuscripts are published online shortly after acceptance, before technical editing, formatting and proof reading. Using this free service, authors can make their results available to the community, in citable form, before we publish the edited article. We will replace this Accepted Manuscript with the edited and formatted Advance Article as soon as it is available.

You can find more information about Accepted Manuscripts in the Information for Authors.

Please note that technical editing may introduce minor changes to the text and/or graphics, which may alter content. The journal's standard Terms & Conditions and the Ethical guidelines still apply. In no event shall the Royal Society of Chemistry be held responsible for any errors or omissions in this Accepted Manuscript or any consequences arising from the use of any information it contains.

ROYAL SOCIETY OF CHEMISTRY

Sustainability Spotlight Statement

View Article Online
DOI: 10.1039/D5SU00525F

Water purification by biocarbon materials is achieving great interest due to their peculiar characteristics such as environmentally friendly nature, easy processability, low cost, natural abundance, high efficiency, etc. to name a few. Biocarbon-based water purification is a sustainable process as the biocarbon based membranes are easily biodegradable and causes no harm to the nature, which helps in the current and future drinking water standards without producing hazardous wastes thus helps in circular economy. Biocarbon-based water purification is a green process under the umbrella of the goals set by the United Nations for a greener future, particularly, Sustainable Development Goal 6: Clean Water and Sanitation.

Open Access Article. Published on 20 November 2025. Downloaded on 12/25/2025 12:38:03 AM.
This article is licensed under a Creative Commons Attribution-NonCommercial 3.0 Unported Licence.

RSC Sustainability Accepted Manuscript

Biocarbon for Sustainable Water purification

View Article Online
DOI: 10.1039/D5SU00525F

Susmi Anna Thomas[1*], Jayesh Cherusseri[2], Asheesh Kumar[3], and Deepthi N. Rajendran[1]

[1]Department of Physics, Government College for Women (Affiliated to University of Kerala), Thiruvananthapuram, Kerala 695014, India

[2]Department of Chemistry (BK21 FOUR), Research Institute of Advanced Chemistry, Gyeongsang National University, Jinju 52828, Republic of Korea

[3]Department of Mechanical Engineering, Mahatma Gandhi Institute of Technology, Hyderabad 500075, Telangana, India

***Corresponding Author**

E-Mail Address: susmithomas123@gmail.com (Susmi Anna Thomas); drjayeshpuli@gmail.com (Jayesh Cherusseri)

Open Access Article. Published on 20 November 2025. Downloaded on 12/25/2025 12:38:03 AM.
This article is licensed under a Creative Commons Attribution-NonCommercial 3.0 Unported Licence.

RSC Sustainability Accepted Manuscript

Abstract

Global environmental challenges including environmental pollution, water scarcity, climate change, are the nightmares to the standard of living for humans on Earth. Research and development in the field of water research paved the way to utilize sustainable materials for water purification and the currently available innovative technologies are capable to purify the water as per the World Health Organization standard. However, the cost of such technologies is very high so that the global population can't accept it. Environmentally friendly and biodegradable materials are highly demanded for water purification. In this context, biocarbon is a suitable material, which exhibits peculiar properties such as low-cost, naturally abundant,

View Article Online
DOI: 10.1039/D5SU00525F

Open Access Article. Published on 20 November 2025. Downloaded on 12/25/2025 12:38:03 AM.
This article is licensed under a Creative Commons Attribution-NonCommercial 3.0 Unported Licence.

RSC Sustainability Accepted Manuscript

eco-friendly, easy to process, etc. As per the *Sustainable Development Goals* set by the United Nations', the SDG: 6 deals with Clean Water and Sanitation. A suitable solution for global freshwater requirement by purifying the contaminated water resources using biocarbon achieved great interest in the recent past. A review report in the field of biocarbon-based water purification is lacking in the literature, which has motivated us to write this review on biocarbon-based water purification. We discuss the synthesis, properties, and water remediation measures of eco-friendly biocarbon and other biocarbon-based materials. This review opens up a new paradigm shift in the water purification technologies which are sustainable, eco-friendly and cost-effective when compared to that of the available technologies.

Keywords: Biocarbon, Water purification, Sustainable material, Circular economy, Green synthesis

1. Introduction

Every country around the globe is now striving for achieving internationally adopted sustainable development goals (SDGs) implemented by the United Nations' (UN) [1, 2]. Exploring technology's role in winning SDGs hold critical factors for decision makers and it facilitates them for overcoming any of the possible trade-marks. The report introduced by the UN says that freshwater requirement is a global challenge in the 21st century. One of the equally important goals in SDGs is wastewater purification [3, 4]. The main contribution was introduced from their capability to increase the availability of water (SDG 6: clean water and sanitation), thereby it facilitates human health in worldwide (SDG 3: good health and for the wellbeing), converting the waste sources towards clean energy (SDG 7: clean and affordable energy) and a reduction in environmental impact from wastewater (SDG 11: sustainable cities

View Article Online
DOI: 10.1039/D5SU00525F

and communities; SDG 12: responsible consumption and its production, SDG 13: climate action and SDG 14:life below water) [5, 6]. The scarcity in pure water for human beings is mainly due to the contamination of pure water and reduction in availability of pure water resources [7, 8]. Wastewater emerges from different activities including households, industrial and agriculture having higher hydraulic load with diverse composition [9, 10]. Effluents from different sectors contain nitrogenous organics, organic carbon, dissolved/suspended solids, inorganics and heavy metal components [11, 12]. Aerosols introduced from the wastewater treatment process transfers infectious agents. These aerosolized droplets present in contaminated wastewater are mainly responsible for spreading SARS-CoV-2 viral infection in a large number of people living in China [13]. The SARS-CoV-2 present in wastewater is recorded and it is given an alert for potential risk transmission of virus by wastewater, having special focus on workers in the field of wastewater/water treatment plants [14, 15]. Additionally, this wastewater transfers many diseases, such as, many people die every year due to the cholera, dysentery, typhoid and other types of diarrheal diseases introduced by poor methods of sanitation [16, 17]. Thus, disposal in an uncontrollable way of untreated wastewater into water resources is associated with prominent impacts of hazardous conditions on the environment and for the human being. The hurdles toward wastewater are heterogeneity and complexity of pollutants which result in the necessity of extraordinary technologies for meeting required standards to the quality of water [18]. The SDGs goals introduced by UNs tends to be universal and it holds equitable accessibility for affordable and safe drinking water by the year of 2030 [19].

The emerging pollutants present in wastewater streams fundamentally contain chemical substances which are non-biodegradable persisting in the environment for a long duration [20, 21]. These pollutants are tending to be spread in the entire food web, which presents potential risk for human health and in environmental ecosystem. Additionally, this pose makes a threat

Open Access Article. Published on 20 November 2025. Downloaded on 12/25/2025 12:38:03 AM.
This article is licensed under a Creative Commons Attribution-NonCommercial 3.0 Unported Licence.

RSC Sustainability Accepted Manuscript

View Article Online
DOI: 10.1039/D5SU00525F

Open Access Article. Published on 20 November 2025. Downloaded on 12/25/2025 12:38:03 AM.
This article is licensed under a Creative Commons Attribution-NonCommercial 3.0 Unported Licence.

for flora-fauna and for other organic species inhabiting the environment [22, 23]. The statistics by the UN shows that effort to attains this SDG goal is slow in many of the countries. In accordance to UNESCO, about 70% of industrial effluents originated in developing countries are untreated and it is dumped [24]. The life cycle assessment and environmental impact quantification and water footprint are major factors for addressing sustainability introduced for establishing consumption/production elements, pollution threats and major depletion of natural resources [25]. The studies relating to wastewater treatment plants utilize various assessments for instruments such as environmental impact quantification, life cycle assessment and gray water footprint for supporting water management stakeholders [26]. There are so many research studies going around the globe for finding a better solution for improving water quality in a sustainable and cost-effective way [27, 28]. The wastewater management develops different avenues for life cycle assessment, environmental impact quantification and gray water footprint for supporting stakeholders in waste management. The wastewater management introduces different avenues for circular economy and develops new and novel business models due to their recovery/reuse of the useful by-products [29, 30]. However, majority of the countries are tightening its regulatory framework, these industries facing hurdles for meeting to discharge water stringent and for requirements of reuse [31]. The industrialization and urbanisation were prominently contributed for adversely impacting society and the environment. As a result, several problems are provoked to manage on a broad level. Conventional procedures for removing heavy metal contaminants from wastewater include precipitation, ion exchange and flotation [32]. But these processes have various drawbacks like their higher energy consumption, reduced removal efficiency and introduction of toxic sludge, which limits its wide range of application [33]. Recently, different alternative treatment routes are studied to improve the quality of treated effluent. This includes desalination, membrane separation, photocatalysis and electrotechnology [31]. The methods implemented for the

RSC Sustainability Accepted Manuscript

View Article Online
DOI: 10.1039/D5SU00525F

Open Access Article. Published on 20 November 2025. Downloaded on 12/25/2025 12:38:03 AM.
This article is licensed under a Creative Commons Attribution-NonCommercial 3.0 Unported Licence.

RSC Sustainability Accepted Manuscript

treatment of wastewater depends upon the material used for it. By searching for various materials having industrial relevance, the researchers implemented the feasibility of nanotechnology for this [34].

Nanotechnology based materials and routes have cutting-edge focus on the introduction of materials for treating polluted water [35]. This procedure involves using nanoparticles or other nano-substances for eliminating pollutants such as inorganic substance, pathogens and organic substances. Among these various materials, carbonaceous components have prominent influence due to its excellent physiochemical properties [36]. In accordance with the prominent demand for sustainable materials having prominent properties and with respect to the beneficial influence for climate change action, sustainable and renewable feedstock like plastic wastes and biomass have a superior role [37]. Among this various sustainable and biocompatible materials, biomass derived carbon, in short, biocarbon have significant influence for wastewater purification due to their abundance, diversity, carbon-rich constituents and with their environmental beneficial facts [38]. Biocarbon have a diverse range of morphological and structural features, yielding it with different physiochemical characteristics and functionality [39].

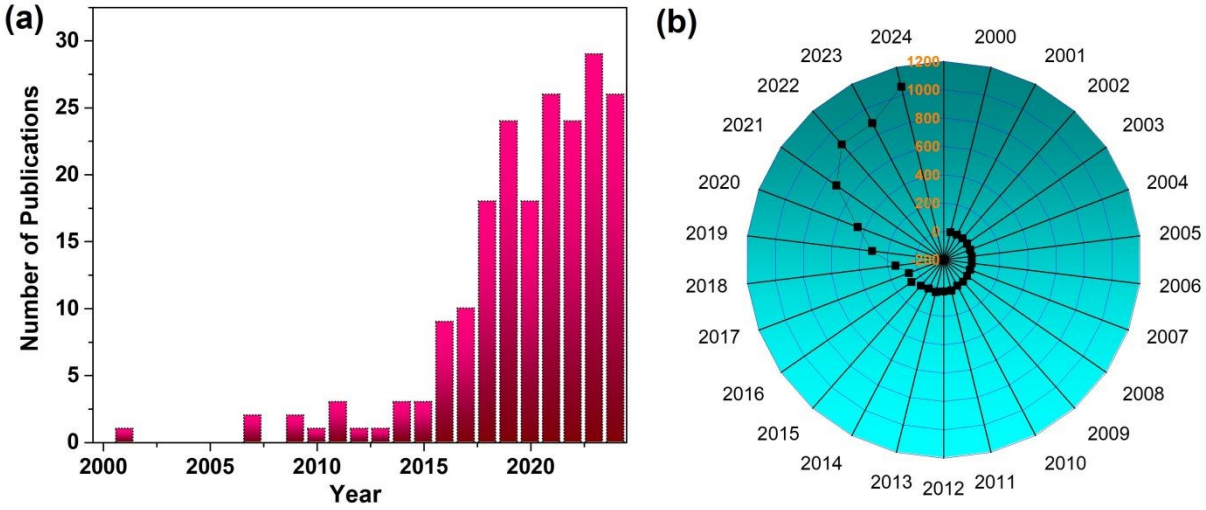

Fig. 1. (a) Number of publications and (b) citations received for the past 25 years based on biocarbon in the literature. [Source: Web of Science, Keyword: "Biocarbon").

View Article Online
DOI: 10.1039/D5SU00525F

Open Access Article. Published on 20 November 2025. Downloaded on 12/25/2025 12:38:03 AM.
This article is licensed under a Creative Commons Attribution-NonCommercial 3.0 Unported Licence.

The carbon related materials have higher dependency to their characteristic features, it is influenced by nature of feedstock and its synthesis method. The various applications require various favourable characteristics [40, 41]. By using bio adsorbent for wastewater treatment, the hydro char/biochar depends upon various properties such as pore size, specific surface area, presence of surface functional groups and their pore volume [42, 43]. The removal efficiency for contaminants by biocarbon materials are effectively influenced by features of contaminants such as its chemical and physical adsorption capacity by it [44]. Generally, biochar synthesized from pyrolysis is prominently recalcitrant and it takes almost a hundred year for their decomposition, thereby it reduces emissions of CO_2 back to the atmosphere and their emissions for carbon is negative [45]. The optimization of physiochemical and optical features of biocarbon materials are necessary to establish it for different fields [46]. The biocarbon materials consists of amorphous carbon structure and graphene sheets which make conductive phase for composites and its antistatic application depends upon processing temperature and the synthesis of biocarbon which provided as an efficient electricity conductor and higher specific surface area hold by material provides reduced loadings sufficient for basic properties which concern thermal, mechanical, optical and contact angle hold by materials [47]. The environmentally friendly biocarbon materials are non-toxic and by character of its reliance on the biological entity for degrading organic and in sometime removing nutrients are vulnerable for toxic contents present in its influent. The huge demand in the field of biocarbon requires a feasible consideration for its availability in large-volume. But detailed review which depicts the features of biocarbon-based materials for wastewater purification is lacking in the literature, especially in the field of new-generation technologies such as desalination, capacitive deionization, etc. The statistical data obtained from the Web of Science are depicted in **Fig. 1** where **Fig. 1a** represents the number of publications and **Fig. 1b** shows the number of citations received for the publication for the past 25 years. This motivated us to present a review based

RSC Sustainability Accepted Manuscript

View Article Online
DOI: 10.1039/D5SU00525F

on novel, new-generation, sustainable and eco-friendly natural biocarbon materials for water purification. This review encompasses an in-depth understanding to the readers on the utilization of biocarbon, especially in waste-water purification. In this current era of sustainability and environmental protection, it is necessary to introduce such sustainable, environmentally friendly, non-toxic and cost-effective biocarbon materials as a futuristic option.

2. Biocarbon for Water Purification

Among different material candidates used for contaminant removal from waste water, adsorption using solid materials, named as adsorbents, tends to be efficient, practical and an easy route [48]. Organic, mineral or biological species adsorb matter. In the past years, there exist various routes which utilize unconventional adsorbents in a more efficient and affordable way for removing contaminants in detectable level [49, 50]. The low-cost materials report in waste-water treatment includes bagasse, agricultural residue, sludge, unburned carbonaceous resources, industrial waste and other materials. Other than these carbonaceous components, metal oxide [51, 52], metal chalcogenides [53, 54], transition metal nitride/carbides [55, 56], etc., are widely used in wastewater purification, especially in desalination. Among these various materials, the biocarbon based materials are used for waste water purification especially due to its features such as porous architecture and a larger surface area. Additionally, it holds favourable parameters like longer stability, hydrophobicity and distinct composition of chemical components [39, 57]. The stable carbon matrix facilitates efficient carbon sequestration and the removal of pollutants from environment for a longer period [58, 59]. The physiochemical features in biocarbon materials can be possible to make a further tuning into a parameter like multifaceted material, it is not only capable in removal of pollutants but it facilitates mineralization acting as catalyst or reducing it to easily-degradable, less toxic

Open Access Article. Published on 20 November 2025. Downloaded on 12/25/2025 12:38:03 AM.
This article is licensed under a Creative Commons Attribution-NonCommercial 3.0 Unported Licence.

RSC Sustainability Accepted Manuscript

View Article Online
DOI: 10.1039/D5SU00525F

byproducts. This prevents pollutant transfer from one to another, like in the membrane separation process [60, 61].

Li et al. have adopted a carbonization procedure on cellulose aerogel in order to synthesize biocarbon aerogel having high porosity, higher specific surface area and reduced density as raw materials for addressing the freshwater requirement by water purification [62]. The preparation method involves modification of nanocellulose using vinyltrimethoxysilane (VTMS), it not only improves mechanical feature of cellulose aerogel through cross-linking, but it catalyses carbonization at a high temperature for increasing carbon residue. The mechanical properties, conductivity and hydrophilicity of biocarbon aerogels tend to be enhanced simultaneously after introducing conducting polymer as an in-situ support. Here, the authors used polypyrrole (PPy) as conducting polymer due to their improved electrical conductivity and a light-to-heat conversion characteristic. A schematic representation of the synthesis method is shown in **Fig. 2**.

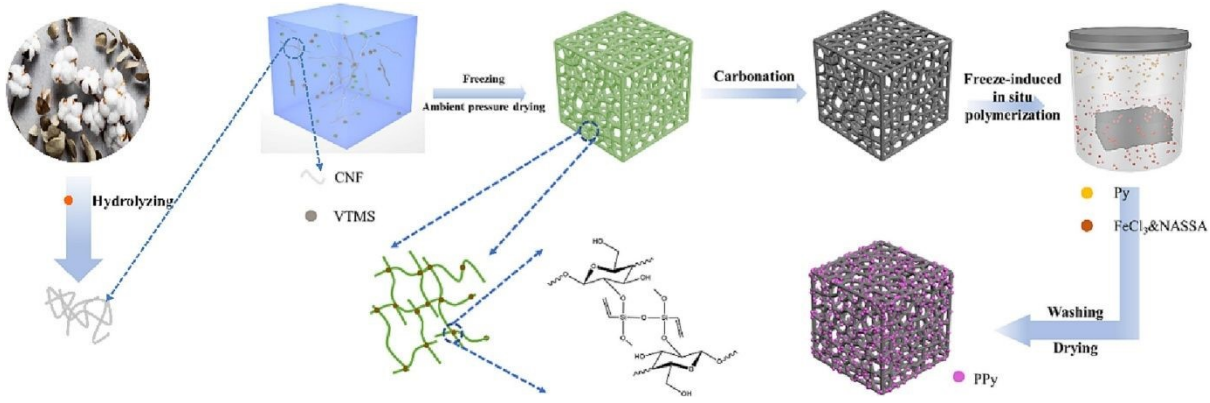

Fig. 2. Schematic representation of CVCAs-P synthesis. Reproduced with permission from [62] Copyright (2023) Elsevier Inc.

By combining a solvent exchange reaction of low surface area, the capillary pressure while solvent evaporation tends to be reduced and biocarbon aerogels are able to dry at an ambient pressure without any shrinkage. In comparison with freeze drying and a supercritical drying

Open Access Article. Published on 20 November 2025. Downloaded on 12/25/2025 12:38:03 AM.
This article is licensed under a Creative Commons Attribution-NonCommercial 3.0 Unported Licence.

RSC Sustainability Accepted Manuscript

View Article Online
DOI: 10.1039/D3SU00525F

Open Access Article. Published on 20 November 2025. Downloaded on 12/25/2025 12:38:03 AM.
This article is licensed under a Creative Commons Attribution-NonCommercial 3.0 Unported Licence.

procedure, the atmospheric pressure drying route is an energy efficient and a low-cost strategy. The morphological characteristics of cellulose nanofiber with VTMS carbon aerogel (CVCAs) and coated with PPy (CVCAs-P) was evaluated through FESEM analysis. Unlike cellulose freeze-dried aerogel-related biocarbon aerogel that possess a porous structure, the CVCAs-P holds a porous with high degree of interconnected laminar architecture having plenty of nanofiber in it (**Fig. 3 a**). The nanofiber diameter is in the range of 480 nm. It is due to the VTMS chemical cross-linking and solvent procedure that efficiently reduce hydrogen link occur between CNFs, through weakening aggregation of nanofiber. Additionally, in the SEM enlarged image (**Fig. 3 b**), it is found that the nanosphere layer is coated on a biocarbon aerogel skeleton, which is corresponding to PPy coated in it. The chemical structure evolution on this samples while synthesis is studied through Fourier transform spectroscopy, as given in **Fig. 3c**. Despite cellulose nanofiber aerogel (CAs), the proposed VCAs have distinct absorption peaks at a wavenumber 760 cm^{-1}, which is obtained through the stretching vibration introduced by Si-O by cross-linking VTMS and CNF. Also, the peaks at a wavenumber 1408 and 1600 cm^{-1} are by the stretching vibrations from vinyl, which represents efficient cross-linking reaction between VTMS and CNF. The absorption intensity for CVCAs was lower to that of VCAs, due to the decomposition of cellulose while carbonization, which results in the removal of a large number of groups. In comparison with CVCAs-P, which shows N-H bond stretching vibration peak present at 1038 cm^{-1} and the C-N-C bond present at the peak position 1166 cm^{-1}, demonstrates successful coating of PPy on CVCAs framework. From thermogravimetric analysis (TGA) shown in **Fig. 3d**, the authors observed that all samples possess a weight loss around a temperature of 100ºC, due to evaporation by weakly bounded water molecules.

RSC Sustainability Accepted Manuscript

View Article Online
DOI: 10.1039/D5SU00525F

Open Access Article. Published on 20 November 2025. Downloaded on 12/25/2025 12:38:03 AM.
This article is licensed under a Creative Commons Attribution-NonCommercial 3.0 Unported Licence.

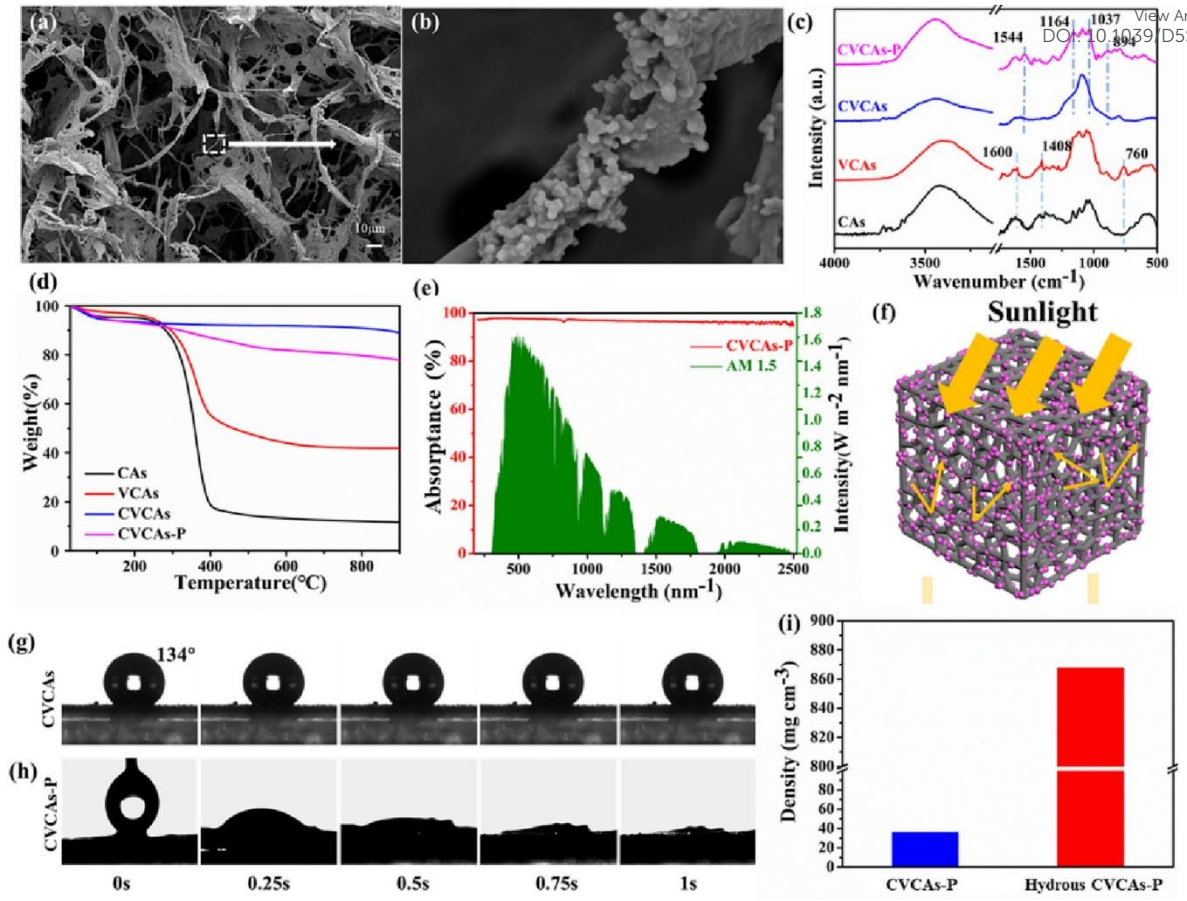

Fig. 3. (a,b) SEM images for CVCAs-P; (c) FTIR spectra and (d) TGA curves for CAs, VCAs, CVCAs and CVCAs-P; (e) solar and absorption spectrum for CVCAs-P; (f) pictorial representation of CVCAs-P light absorption; Dynamic contact angle of water for (g) CVCA-s and (h) CVCAs-P; (i) density value before and after absorption of water in the case of CVCAs-P. Reproduced with permission from [62] Copyright (2023) Elsevier Inc.

The onset value corresponding to thermal degradation (T_{onset}) and temperature for maximum degradation rate (T_{max}) for CAs is obtained to be 260 and 360ºC, respectively. In the case of VCAs, T_{onset} and T_{max} is calculated as 220 and 363ºC and it is lower than that of CAs. In fact, VTMS as a silicon-contain molecule provides dehydration of cellulose and their carbonization at a low temperature. More specifically, residual quantity (about 42%) of VCAs is much greater than CAs (11%) which demonstrates that addition of VTMS prominently make a transformation of cellulose towards stable carbon and it increase rigidity and the mechanical

RSC Sustainability Accepted Manuscript

View Article Online
DOI: 10.1039/D5SU00525F

properties of CVCAs, it is favourable to withstand maximum value of about 500 times of its own weight by mechanical load-bearing study in water. In accordance with the thermal conductivity analysis, the authors of this work obtained a thermal conductivity of 0.32 W mK^{-1} in the case of CVCAs-P. After coating PPy, there occurs a degradation in PPy, having weight loss in the range of 260-540ºC. This obtained results accomplishes the successful preparation of porous nanocellulose-related biocarbon aerogel having high retention in weight. In order to utilize the prepared materials as photo-thermal conversion candidates, the authors of this work taken diffusion reflection spectrum and transmission spectrum using UV-Vis-NIR spectrophotometer. From this spectrum, it is observed that diffuse reflectance and transmission stays below 4% and 2%, respectively. The CVCAs-P absorption spectrum was calculated and given in **Fig. 3e**. The CVCAs-P possess a wide range for solar absorption band and it absorbs light energy present in sunlight having efficiency of light absorption in the range of 94-97% and it efficiently absorb light energy, which provides theoretical base to the CVCAs-P study with excellent performance features for photo-thermal conversion. The sunlight absorption in CVCAs-P was represented with a diagram given in **Fig. 3f**. Due to 3D porous structure in CVCAs-P, there exists a higher number of voids which provides sunlight in the interior portion of CVCAs-P, if it is effectively irradiated. Additionally, due to the irregular linear structure present inside the CVCAs-P, sunlight makes a continuous reflection inside CVCAs-P, eventually the majority of it tends to be absorbed and a smaller portion escapes to the outer portion. The efficiency in light absorption by CVCAs-P is greater than majority of currently available photo-thermal conversion material like poly-methylmethacrylate (PMMA), graphene oxide (GO), Si/PPy–polyvinyl alcohol, Ti_2O_3, janus graphene membrane, PDA (polydopamine)@Ag nanoparticles, copper foam, dual-phase molybdenum nitride nano rambutan, all carbon nanotube (CNT) hybrid film. In comparison with obtained results, the CVCAs-P have high

Open Access Article. Published on 20 November 2025. Downloaded on 12/25/2025 12:38:03 AM.
This article is licensed under a Creative Commons Attribution-NonCommercial 3.0 Unported Licence.

RSC Sustainability Accepted Manuscript

View Article Online
DOI: 10.1039/D5SU00525F

efficiency for light absorption. The hydrophilic features are prominent as photo-thermal material for water purification. With respect to the hydrophilic group loss in treatment procedure, the CVCAs have hydrophilic features with water contact angle in the range of 134º and there exists a barely change for water contact angle after 1s (**Fig. 3g**). This would make a reduction in rate of water transfer and the efficiency for treatment. After the PPy coating, the aerogel surface turned to hydrophilic phase from hydrophobic, as proven by the fact that water droplets make a total absorption within 1s, as shown in **Fig. 3h**. As given in **Fig. 3i**, the density value of hydrous CVCAs-P reaches to 867.7 mg cm^{-3} and absorption rate of water reaches to 23.1 gg^{-1}, which is found to be 23.1 times of their mass. This proposed result indicates that CVCAs-P is efficient for higher rate of water transfer. The authors of this work evaluated the change in surface temperature value of water and CVCAs-P under the presence of light using infrared thermography (IR). The authors of this work observed that there exists a rise in water surface temperature from 20.3ºC to 25.4ºC in a time duration of 30 minutes for 1 sun, with an increase only a range of 5.1ºC. On the other hand, the temperature value of CVCAs-P from a temperature 21.1ºC to 34.9ºC for a time duration of 30-minute increases to 13.8ºC and it is greater than pure water. This prominent difference in temperature is due to the higher efficiency of light absorption by CVCAs-P, it provides faster absorption and a conversion of sunlight to heat by the use of energy conversion. Through mass change evaluation, the authors of this work found that the evaporation rate value of both pristine and CVCAs-P treated with water introduced a dramatic increase for the first 5 minute after receiving light. After 20-minutes, the apparent evaporation rate of pure water was stable at a value 0.34 kg m^{-2} h^{-1}. Here low surface temperature limiting evaporation of water is through the limit in absorption capacity of light, which only provides small percentage in conversion of light energy to heat. On the other hand, the apparent value of water evaporation rate by CVCAs-P is higher as 1.53 kg m^{-2} h^{-1}. It occurs due to higher light absorption capability of CVCAs-P, which makes an efficient sunlight

Open Access Article. Published on 20 November 2025. Downloaded on 12/25/2025 12:38:03 AM.
This article is licensed under a Creative Commons Attribution-NonCommercial 3.0 Unported Licence.

RSC Sustainability Accepted Manuscript

View Article Online
DOI: 10.1039/D5SU00525F

Open Access Article. Published on 20 November 2025. Downloaded on 12/25/2025 12:38:03 AM.
This article is licensed under a Creative Commons Attribution-NonCommercial 3.0 Unported Licence.

absorption and excellent conversion capability for photo-thermal reaction, it makes a rapid conversion of light energy absorbed to heat energy and for heating water. Additionally, due to the efficient hydrophilicity rate of CVCAs-P, water makes a continuous transfer to evaporating surface which escapes using porous mesh like architecture. To establish evaporation rate of CVCAs-P at high sunlight intensity, the intensity value of simulated Xe lamp is adjusted to 2, 3, and 4 kW m^{-2} for 2, 3 and 4 sun, respectively, at a room temperature and humidity range of 21±0.5ºC and 40-42%, respectively. The evaporation capacity for water in the presence of 2, 3, and 4 sun is observed to be greater than 1 sun, as high intensity sunlight facilitates more light energy. Here the surface of evaporation has a more prominent temperature through absorption of light and photo-thermal conversion features of CVCAs-P. As the temperature value of evaporation surface increase, water molecule movement is highly intense, which results in a high evaporation rate. The evaporation rate of water held by CVCAs-P is maintained at 1.53-1.59 kg m^{-2} h^{-1} for the 30 repetitions, it proves efficient cyclic stability of CVCAs-P and it is possible to reuse many times. Additionally, the authors of this work evaluated the chemical stability by immersing CVCAs-P in strong NaOH solution acid and in strong HCl solution base for a duration of 8 h. It is found that CVCAs-P appearance doesn't make a change after acid or base treatment. Here, CVCAs-P treated by strong acid and base is washed and it is separately tested for evaporation. It is found that change in mass and evaporation rate curve obtained for CVCAs-P treated with HCl is almost similar with that of untreated CVCAs-P. Apparent evaporation rate of water is upto 1.54 kg m^{-2} h^{-1} by a minus evaporation rate of water under dark (0.17 kg m^{-2} h^{-1}) gives resultant evaporation rate of 1.37 kg m^{-2} h^{-1}, it is less than theoretical limit 1.47 kg m^{-2} h^{-1}. Beside of this, the apparent evaporation rate of water in CVCAs-P having NaOH treated was reduced to a value 1.32 kg m^{-2} h^{-1}, it is due to the influence from NaOH on PPy, the protonation and the de-doping by PPy in alkaline atmosphere and disruption of large conjugated architecture in PPy. After performing treatment for a

RSC Sustainability Accepted Manuscript

View Article Online
DOI: 10.1039/D5SU00525F

duration of 28 days under alkaline atmosphere, CVCAs-P still maintains a capacity of 1.24 kg m^{-2} h^{-1} under water treatment, and it maintains for 80%. This proposed experiment reveals that CVCAs-P is observed to be tolerant towards strong acid and it is adapted for utilization in a high acidic environment. Introducing salt ions provides a small quantity of crystallization on material by evaporation of water, which reduces rate for water transportation. To evaluate the utilization of CVCAs-P in the practical purpose of water purification, the authors of this work used lake water for producing purified water. Through optical microscopy image analysis for untreated lake water, the authors of this work observed a large number of microorganisms, but in purified water there is no microorganism after CVCAs-P treatment. In the photothermal purification of water through materials, their dependency to sunlight is a serious concern, it is considered to be a bottleneck in wide range of application. To establish steam generation in all-weather conditions, it is necessary to introduce electro-thermal conversion route in order to ensure steam may still need to generate in absence of the light or in poor light. A classical electro-thermal phenomena procedure needs efficient electrical conductivity for ensuring that low voltage input introduce adequate heat for the production of steam. The value of electrical conductivity hold by CVCAs-P was reached to 0.79 S m^{-1}, it is attributed to linear structure in CVCAs it acts as a more conductive junction than traditional honeycomb architecture, which facilitates higher conductive pathway in CVCAs and this network architecture provides electric current transmission on CVCAs in extremely faster way. In compared with CVCAs, conductivity value of CVCAs-P increases to a more doubled value, which attains 1.95 S m^{-1}, it is due to the efficient loading of PPy onto surface of CVCAs skeleton as conducting polymer, thus it widens the conducting route. Secondly, PPy is a conjugated polymer and double doping by carboxyl group and sulfonic acid in NASSA provides a more conjugated extensive system as a conductive channel, which improves PPy conductivity, thereby increase conductivity for CVCAs-P. It is possible to evaluate water evaporation through electrical conversion from

Open Access Article. Published on 20 November 2025. Downloaded on 12/25/2025 12:38:03 AM.
This article is licensed under a Creative Commons Attribution-NonCommercial 3.0 Unported Licence.

RSC Sustainability Accepted Manuscript

View Article Online
DOI: 10.1039/D5SU00525F

externally connected power supply at night, through synergistic influence of photo-thermal and electrical heating in overcast or cloud condition or through heating of photo-thermal in case of sunny atmosphere, thus it enable all-weather evaporation of water. The conceptual diagram for water treatment of all-weather related CVCAs-P is shown in **Fig. 4a**. The CVCAs-P surface temperature attains 23.1ºC and water evaporation apparent rate reached to 0.20 kg m^{-2} h^{-1} in presence of only about 1 V, which represents evaporation of water at the night condition by CVCAs-P (shown in **Fig. 4b** and **c**). Here temperature of surface and their water evaporation apparent rate for CVCAs-P was tested for 0.5 sun and 1V and the authors of this work obtained a surface temperature of 28.7ºC and an apparent water evaporation rate as 0.78 kg m^{-2} h^{-1}, respectively. There exists an increase in temperature as 1.8ºC and water evaporation apparent rate increases to 0.12 kg m^{-2} h^{-1}, in compared with 0.5 sunlight irradiation, which demonstrates the efficiency of CVCAs-P for water evaporation through synergistic photo-thermal and in electro-chemical means.

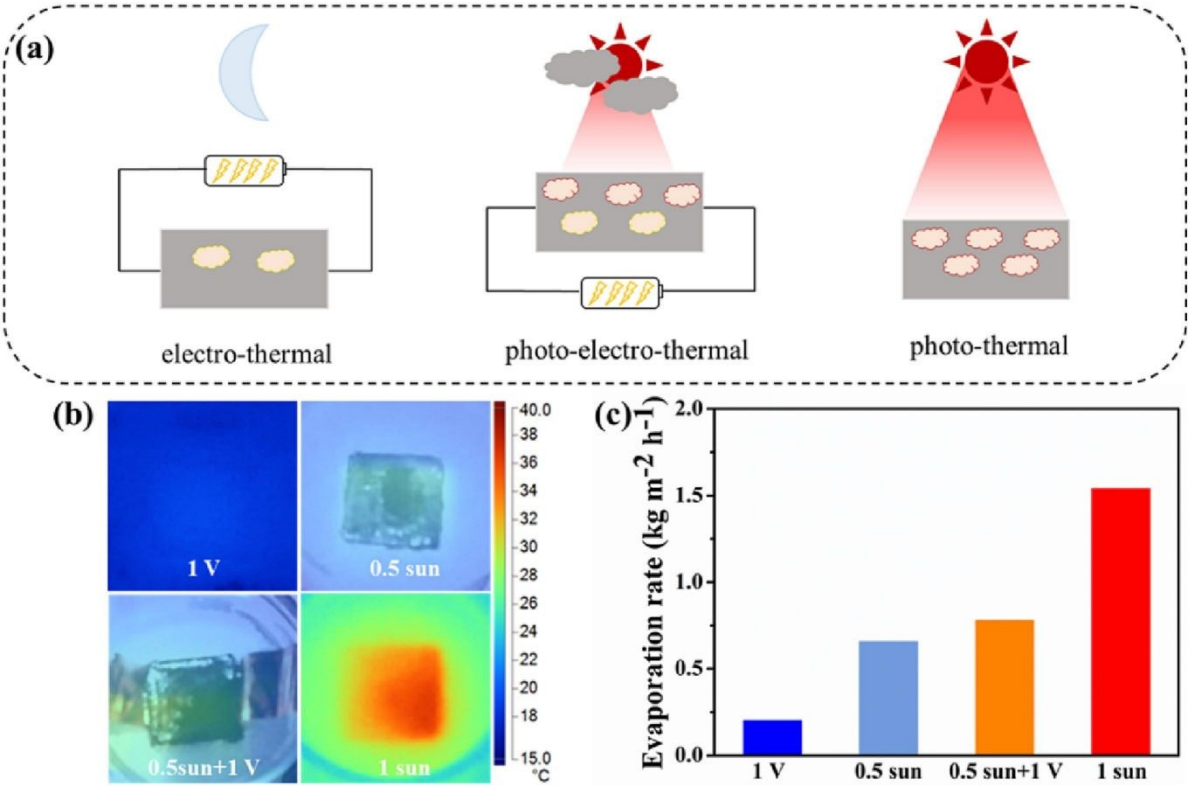

Open Access Article. Published on 20 November 2025. Downloaded on 12/25/2025 12:38:03 AM.
This article is licensed under a Creative Commons Attribution-NonCommercial 3.0 Unported Licence.

RSC Sustainability Accepted Manuscript

View Article Online
DOI: 10.1039/D5SU00525F

Fig. 4. Concept diagram for (a) all-weather treatment, (b) surface temperature and (c) apparent evaporation rate of water in the case of CVCAs-P at 1 V, 0.5 sun, 0.5 sun+1 V and 1 sun, respectively. Reproduced with permission from [62] Copyright (2023) Elsevier Inc.

Open Access Article. Published on 20 November 2025. Downloaded on 12/25/2025 12:38:03 AM.
This article is licensed under a Creative Commons Attribution-NonCommercial 3.0 Unported Licence.

There is a work based on the utilization of biocarbon particles for the formaldehyde removal. Here the authors synthesized biocarbon samples from olive stone and Arundo donax feedstocks for various pyrolysis temperatures ranging from 300 to 800ºC. Through FTIR spectra, the authors of this work observed that spectra corresponding to both the synthesized biomass samples revealed the appearance of peaks in same positions. Additionally, there exists diverse functional groups for biomass sample prepared at low temperature (less than 500ºC) regardless of the type of biomass. By increasing the pyrolysis temperature, there exists a reduction in O-H polar stretching corresponding to hydroxyl group, it is related to the evaporation of water besides alcohol and carboxyl group degradation. The carboxyl group degradation was correlated with the reduction obtained for acidity of biocarbon at a high temperature. The authors of this work observed that structural and physiochemical features are depends upon pyrolysis temperature where this biocarbon is synthesized. Through various analyses, the authors of this work found that there exists an increase in the hydrophobicity, pH and porosity features of biocarbon with respect to the increase in pyrolysis temperature. The authors of this work obtained a removal capacity for formaldehyde in the range of 26% and 64% for samples synthesized at temperatures of 300 and 800ºC, respectively. Here, for the biocarbon pyrolysis done at a temperature under 500ºC, the capture of formaldehyde is governed through the partitioning mechanism of diffusion in nanocarbonized organic fraction. For a comparison, the capture of formaldehyde is controlled with physical adsorption phenomena by pore filling of biocarbon pyrolyzed at a temperature of 500ºC or above. The authors of this work found that biocarbon pyrolyzed for a temperature of 800ºC is highly effective for adsorption of

RSC Sustainability Accepted Manuscript

View Article Online
DOI: 10.1039/D5SU00525F

formaldehyde due to perfectly developed microporous architecture in both the Arundo donax and olive stone. The authors of this work used Arundo donax-derived biocarbon synthesized at a temperature of 800ºC for reusability test, via thermal regeneration for the removal of adsorbed components. This sample regenerated hold a comparable removal capacity for formaldehyde upto four reusable cycles. The authors found that comparison between activated and non-activated Arundo donax biomass reveals physical activation which prominently enhances adsorptive capability of biocarbon[63]. A novel composite of NiHCF/NSBC was synthesized through combination of nickel hexacyanoferrate (NiHCF) having co-doped by nitrogen (N) and sulfur (S) in biocarbon (NSBC) synthesized from coconut shells for the removal of toxic pharmaceutical contaminants amoxicillin and ciprofloxacin present in the aquatic systems. The authors of this work utilized a multi-step procedure for the synthesize of this bio-carbon co-doped system from coconut shell. In the first step, the authors of this work extensively rinsed the coconut shell with water for the removal of impurity and dried at a temperature of 100ºC for a duration of 24 h. The raw biocarbon was produced through subjecting desiccated shells for pyrolysis at a temperature of 500 ºC for a time duration of 3 h in N_2 atmosphere. Then the authors of this work crushed and kept sieving for ensure a uniformity in particle size. The authors of this work performed doping by dissolving urea and thiourea in deionized water at 1:1 M ratio. The impregnated biocarbon was kept for drying at a temperature of 80 ºC for a duration of 12 h before performing calcination at a temperature of 600 ºC for a duration of 2 h in N_2 environment for achieving co-doping with N and S. The authors of this work labelled the resultant doped biocarbon collected as NSBC. For the synthesize of NiHCF, the authors of this work used a co-precipitation approach. For this, the authors of this work have dissolved nickel nitrate hexahydrate in deionized water and kept for stirring through ultrasonication by adding potassium ferricyanide solution. The resultant precipitate was kept for centrifugation and washed with deionized water for removing impurities and kept for drying. This resultant

Open Access Article. Published on 20 November 2025. Downloaded on 12/25/2025 12:38:03 AM.
This article is licensed under a Creative Commons Attribution-NonCommercial 3.0 Unported Licence.

RSC Sustainability Accepted Manuscript

View Article Online
DOI: 10.1039/D5SU00525F

Open Access Article. Published on 20 November 2025. Downloaded on 12/25/2025 12:38:03 AM.
This article is licensed under a Creative Commons Attribution-NonCommercial 3.0 Unported Licence.

NiHCF product is used for the preparation of hybrid NiHCF/NSBC composite. Similarly, the authors of this work prepared NiHCF/NSBC composite through dispersing NSBC in deionized water by ultrasonication and the resultant NSBC suspension is treated using NiHCF pre-synthesized and mixture is tired continuously for 6 h. The obtained slurry is desiccated at a time duration of 80 ºC for 12 h and kept for calcination at a time period of 400 ºC for 2 h in N_2 atmosphere. The finally obtained hybrid NiHCF/NSBC composite was collected and the authors of this work labelled it as NiHCF/NSBC. The authors of this work have taken the FTIR spectra for prepared NSBC, NiHC and its hybrid composite for evaluating the functional groups present in it. The NiHCF peak present at 2102 cm^{-1} represents stretching vibration from cyanide group, it is the prominent characteristic feature of counterpart Prussian blue (PB) structure. The signal present at a wavenumber 1655 cm^{-1} is through bending of H-O-H vibration, which represents the appearance of water molecules. The peak present at 1415 and 1086 cm^{-1} represent stretching vibration from coordinated nitrate ion and Fe-C ≡ N bending vibration. Also, there is a peak present at 745 cm^{-1} which is corresponds to stretching vibration from Ni-N, demonstrating that NiHCF hold structural integrity. The appearance of surface functional group which contribute towards hydrophilicity and the adsorption of pollutant was represented through a broad peak present at 3420 cm^{-1} in the case of NSBC, it is corresponding stretching vibration of O-H in hydroxyl group. While doping procedure, the residual N-contain precursor is likely the reason for sharp peak exists at a wavenumber 2088 cm^{-1} it is attributed to C ≡ N group stretching vibration. The peak present at 1692 cm^{-1} is corresponding to C=O group stretching vibration, which represents the presence of carbonyl functionality. Conversely, peak present at 1480 cm^{-1} represent bending vibration of N-H, which shows the successful doping of nitrogen. The stretching vibration from C=S is responsible for the presence of peak at 1049 cm^{-1}, which confirms S injection into biocarbon matrix. The NSBC acts as an efficient support for hybrid photocatalysts process, due to collective improvement of

RSC Sustainability Accepted Manuscript

View Article Online
DOI: 10.1039/D5SU00525F

their adsorption capacity, electronic features and active sites introduced by functional group. The structural integrity in NiHCF is then confirmed with stretching vibration of Ni-N. The NiHCF/NSBC FTIR spectrum exhibits a substantial alteration in compared with pristine materials, as peak present below 1000 cm^{-1}, tend to be disappeared, which suggests robust interaction between NSBC and NiHCF. The resultant hybrid possesses prominent increase in intensity of cyanide characteristic stretching peak in NiHCF at a wavenumber 2082 cm^{-1}, it represents that NSBC matrix was facilitated with an improved charge transfer and electronic interaction. This modification was verified with efficient hybridization and improved electronic properties of hybrid NiHCF/NSBC, it is corresponding to the prominent photocatalytic characteristics. The authors of this work evaluated the morphological features of prepared samples using SEM and TEM. The NiHCF SEM image shows spherical particles having size in the range of 100-200 nm (**Fig. 5a**).

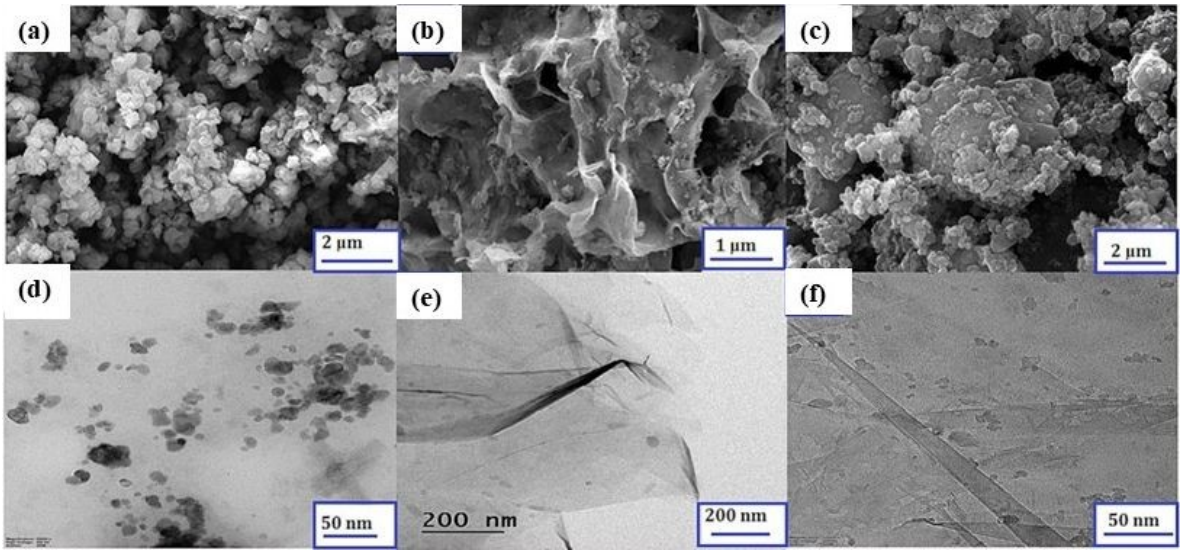

Fig. 5. SEM image of (a) NiHCF, (b) NSBC, and (c) NiHCF/NSBC. TEM image of (d) NiHCF, (e) NSBC and (f) NiHCF/NSBC. Reproduced with permission from [64] Copyright (2025) Elsevier Inc.

Open Access Article. Published on 20 November 2025. Downloaded on 12/25/2025 12:38:03 AM.
This article is licensed under a Creative Commons Attribution-NonCommercial 3.0 Unported Licence.

RSC Sustainability Accepted Manuscript

View Article Online
DOI: 10.1039/D5SU00525F

Open Access Article. Published on 20 November 2025. Downloaded on 12/25/2025 12:38:03 AM.
This article is licensed under a Creative Commons Attribution-NonCommercial 3.0 Unported Licence.

RSC Sustainability Accepted Manuscript

These particles make a dense agglomeration due to intrinsic interparticle interaction and it potentially limits surface functionality, which restricts their utilization in catalytic application. In contrast NSBC sample (**Fig. 5b**) possess sheet-like morphology with irregular and porous architecture, it represents the structural flexibility and high surface area. These given features are advantageous for pollutants adsorption and dispersion of the catalytic particles. The hybrid NiHCF/NSBC composite hold uniform fusion of this morphology, having sphere-like NiHCF uniformly anchored on NSBC sheets (**Fig. 5c**). The proposed configuration makes a simultaneous improvement in stability and dispersion of NiHCF particles while simultaneous reduction in agglomeration. The TEM analysis of NiHCF (**Fig. 5d**) shows spherical particles having distinct edges, which signifies their good crystallinity. Besides of this, particle hold tight clustering, which results to a dense aggregation that could hinders their catalytic efficiency due to restriction in accessibility of their surface. The NSBC (**Fig. 5e**) have sheet-like structure, which is evaluated with pronounced imperfections and folds, which underscore their amorphous composition of carbon. The presence of wrinkles and appearance of porous structure indicates prominently disordered architecture, which augments their capacity to engage in nanoparticle and contaminant. The TEM image corresponding to NiHCF/NSBC (**Fig. 5f**) shows well-defined hybrid architecture having NiHCF particles are affixed uniformly to NSBC sheets. The NiHCF spherical particles demonstrates a reduction in aggregation relative to NiHCF pristine, which signifies their enhanced level of dispersion enabled by NSBC matrix. The sheet structured biocarbon provides strong support, which provides spatial separation between NiHCF particle for confirming optical exposure for the active area. The authors of this work evaluated the optical features of prepared samples using UV-DRS technique and observed a prominent absorption edge in visible spectrum, representing bandgap energy approximately as 2.3 eV. The NSBC have extensive absorption in visible spectrum with respect to doped carbon structure, thereby improves light harvesting. The hybrid NiHCF/NSBC

View Article Online
DOI: 10.1039/D5SU00525F

composite exhibits redshift in absorption edge, which is relative to pristine NiHCF, signifies the reduction in bandgap energy around 1.8 eV. This alteration represents improvement in absorption of visible light resulting from synergistic interaction of NiHCF and N,S-doped biocarbon matrix. The hybrid architecture features light harvesting features of NSBC, which enhance composite efficiency under visible light. The photocatalytic efficiency of NiHCF, NSBC and the hybrid NiHCF/NSBC composite was evaluated with ciprofloxacin degradation in aqueous solution for irradiation of visible light and in UV. In order to exclude the non-photocatalytic degradation, the control experiments are done in the absence of catalyst and without applying light. For optimizing loading of catalyst, the authors of this work performed experiments using 25, 50, 75, and 100 mg catalyst for 100 mL of the 10-ppm ciprofloxacin pollutant solution for identical conditions. It is observed that the degradation is extremely slow for catalyst loading of 25 mg, however, absorption is substantially higher for 75 and 100 mg. By the use of 50 mg catalyst, there exists a moderate photodegradation rate and absorption is observed to be minimal. Thus, the authors of this work used catalyst with 50 mg loading for entire trial. From the UV spectra of ciprofloxacin under different irradiation time indicates absorption peak intensity at a wavelength of 277 nm makes a gradual reduction with respect to the increase in irradiation time due to the photocatalytic efficiency of NiHCF/NSBC composite. The reduction in intensity of absorption verifies that under irradiation of visible light, catalytic action by prepared composite makes efficient breakdown for ciprofloxacin. This composite delivers a degradation efficiency value of 94% for a time duration of 90 minute under visible light, surpassing the NiHCF (73%) and NSBC (78%) under similar condition. This result indicates that proposed hybrid composite holds an efficient separation of charge, absorption of pollutant and light absorption efficiency. Here reduction in degradation efficiency hold by bare NiHCS is by the higher bandgap energy and by rapid recombination of photogenerated charge carrier. On the other hand, NSBC sheet present in prepared composite work as an efficient

Open Access Article. Published on 20 November 2025. Downloaded on 12/25/2025 12:38:03 AM.
This article is licensed under a Creative Commons Attribution-NonCommercial 3.0 Unported Licence.

RSC Sustainability Accepted Manuscript

View Article Online
DOI: 10.1039/D5SU00525F

Open Access Article. Published on 20 November 2025. Downloaded on 12/25/2025 12:38:03 AM.
This article is licensed under a Creative Commons Attribution-NonCommercial 3.0 Unported Licence.

electron acceptor, which allows rapid transfer in photoinduced electron from conduction band in NiHCF to NSBC, provides increase in photocatalytic efficiency by effective separation of charge and its transfer. The faster degradation kinetics represent that synergy between NiHCF and NSBC with an improved adsorption of pollutant and expansion in light absorption range. This proposed result shows that hybrid composite was not only provides an increase in photocatalytic degradation, but a dramatic speed for reaction dynamics in compared with pure equivalents. Similarly, the authors of this work performed degradation analysis for amoxicillin under visible light and found that prepared composite hold a degradation efficiency of 92% in 90 min and it is greater than NiHCF (65%) and NSBC (72%). This proposed degradation analysis results show that prepared hybrid composite is capable for real-world applications by demonstrating that it is not only increase the efficiency of photocatalytic mechanism, but also improves reaction kinetics. For the demonstration of practical application, the authors performed reusability test and obtained a retention of greater than 90% of initial degradation capability for both the pollutants after finishing five cycles. This high retention rate demonstrates the excellent stability of composite, especially due to its structural stability. The authors studied the effect of photocatalytic mechanism introduced by this hybrid composite and given as a schematic in **Fig. 6a**. Under exposure of visible light, the NiHCF makes absorption of photon and it generate e^-/h^+ pair. The electron transferring to NSBC, where it reduces O_2 to O_2^- and holes in valence band of NiHCF oxidizes H_2O/OH^- to OH. This reactive oxygen species tends to degrade pollutants to a non-toxic product like CO_2 and H_2O. The UV results shows that NiHCF pristine has absorption edge correspond to bandgap value of approximately 2.3 eV. The authors of this work found that resultant composite possesses a noticeable range of redshift in absorption edge, which represents improvement in absorption of visible light. The bandgap energy calculated was tend to be decrease to approximately 1.8 eV, which provides efficient utilization of solar spectrum. This redshift is corresponding to the

RSC Sustainability Accepted Manuscript

View Article Online
DOI: 10.1039/D5SU00525F

Open Access Article. Published on 20 November 2025. Downloaded on 12/25/2025 12:38:03 AM.
This article is licensed under a Creative Commons Attribution-NonCommercial 3.0 Unported Licence.

NSBC incorporation, which provides defect level and improve photon harvesting. Additionally, the photoluminescence (PL) spectrum demonstrates that NiHCF pristine displayed string intensity for PL, represents e^-/h^+ rapid recombination. On the other hand, the hybrid composite possess prominently quenched intensity for PL, suggests the excellent separation and a transfer for photogenerated electron due to defect-rich and conductive NSBC matrix. Additionally, interfacial transportation of charge was evaluated through EIS and shown in **Fig. 6b**. With respect to the Nyquist plot, the authors of this work found a prominently narrow semicircular arc in compared with pristine NiHCF and NSBC having low charge transfer resistance (R_{ct}). The S and N doping introduce extra electron path and provides efficient transportation of electron across the composite interface, thereby there exists an increase in conductivity. Additionally, the authors of this work performed photocurrent analysis for analysing the movement and generation of charge carrier under exposure of light, as shown in **Fig. 6c**. This composite has considerably high photocurrent density in compared with individual counterparts, which confirms the generation of more electron and efficient transportation in composite, which supports the enhancement in separation of charge and their photocatalytic efficiency. To identify ROS in photocatalytic degradation, the authors of this work conducted scavenger experiment with benzoquinone (BQ), tert- butanol (TBA) and ethylenediaminetetraacetic acid (EDTA) as a quenching agent for the hydroxyl radical, photogenerated hole and superoxide radical, respectively. By analysing **Fig. 6d**, the authors of this work found that BQ addition results to a prominent drop in efficiency of photodegradation of ciprofloxacin from a range 94 to 48%, which clearly confirms superoxide radical is the major reactive species which take a role as pollutant degradation. By the introduction of TBA, efficiency make a reduction to 74%, which indicates that hydroxyl radical also makes a participation in degradation.

RSC Sustainability Accepted Manuscript

View Article Online
DOI: 10.1039/D5SU00525F

Open Access Article. Published on 20 November 2025. Downloaded on 12/25/2025 12:38:03 AM.
This article is licensed under a Creative Commons Attribution-NonCommercial 3.0 Unported Licence.

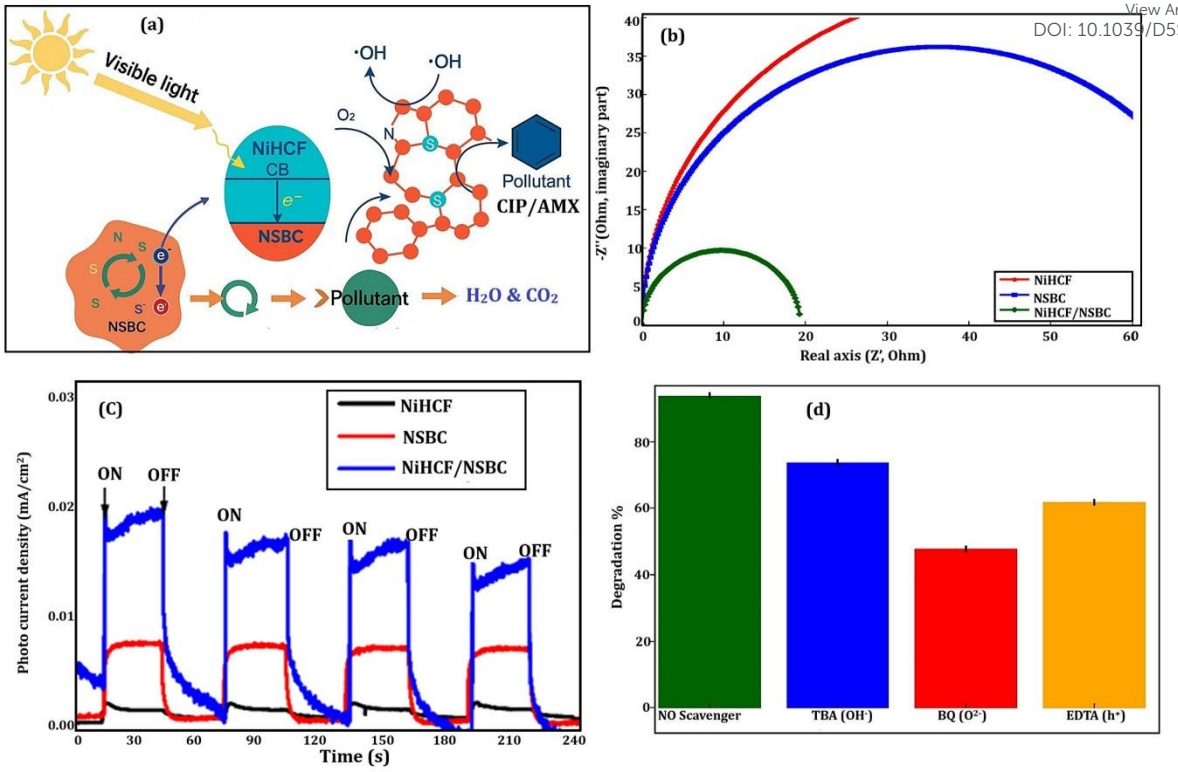

Fig. 6. (a) Mechanism of photocatalysis; (b) Nyquist plots; (c) response of photocurrent; (d) scavenger test. Reproduced with permission from [64] Copyright (2025) Elsevier Inc.

During EDTA presence, which makes a marginal reduction for its efficiency, represents that direct degradation introduced by photogenerated holes induce a limited role. The observed results show that photocatalytic degradation was prominently influenced by O_2^- radical, having OH^- contributes as secondary oxidizing agent. This observation demonstrates the efficient photocatalytic efficiency of composite which is dictated through efficient separation of charge, enhanced absorption of visible light and rapid interfacial transfer of charge. The photocatalytic efficiency was due to synergistic influence from optical, structural and electrochemical characteristics and leads to the efficient tool for pharmaceutical contaminant removal. Using a simple hydrothermal procedure at low-temperature, Zhang et al. [65] efficiently anchored akaganeite (β-FeOOH) nanoparticle on a biocarbon of sea porous buckthorn without applying any surfactants or other external candidates. Here the authors of this work prepared SBC@β-

RSC Sustainability Accepted Manuscript

View Article Online
DOI: 10.1039/D5SU00525F

Open Access Article. Published on 20 November 2025. Downloaded on 12/25/2025 12:38:03 AM.
This article is licensed under a Creative Commons Attribution-NonCommercial 3.0 Unported Licence.

FeOOH using hydrothermal reaction with $FeCl_3.6H_2O$ and urea, where sea buckthorn branches impregnated by $ZnCl_2$ activated agent. Using SEM analysis, the authors found that SBC naked powder have irregular structure with large quantity of pores on their surface. From high-magnification SEM image, the authors of this work found that abundant SBC cavities have diverse diameter with a homogeneous distribution on their surface, which facilities a high surface area for prepared SBC@β-FeOOH composite. With respect to the loading by β-FeOOH fine particle onto SBC scaffold, there exists a topographical rough surface by the resultant composite. The SBC surface is covered by β-FeOOH small particles, however, the porous architecture in parent SBC candidate is maintained, it favours the contaminant adsorption. The existence of cooked phenomena for few pore channels, when compared with SBC original substrate, provides assertive proof that β-FeOOH were surface anchored onto SBC surface scaffold. Additionally, the absence in scattering particle around composite material indicates efficient adhesion between scaffold SBC and β-FeOOH nanoparticle. Using high-magnification image, the authors of this work found that β-FeOOH nanoparticle hold ellipsoidal morphology with smooth surface, which resembles 1D nanorod having width and length in the range of 70-120 and 300-400 nm, respectively. The authors of this work evaluated the absorption efficiency for doxycycline (DC) in fixed bed column procedure which is operated for DC sorption from aqueous solution. This fixed column approach provides efficient utilization of fixed-bed column which allows efficient utilization of sorbent capacity and it results to effluent having high quantity. Additionally, when compared with batch method, the authors of this work utilized a fixed-bed column which allows highly efficient cycles for adsorption/regeneration and it reuse sorbent and ultimately scale-up fixed-bed column from laboratory towards pilot and in industrial scale. Through breakthrough profile analysis, the authors of this work found that there exists a reduction in breakthrough time from 80 to 48 minute, when DC concentration of influent changed from 22 to 32 mg L^{-1} in bed having depth

RSC Sustainability Accepted Manuscript

View Article Online
DOI: 10.1039/D5SU00525F

of 1.1 cm, which is operated at flow rate value of 1 mL min^{-1} having with pH of 6. The accumulation rate of DC in fixed-bed column represented as function of total sorbent mass in column. There exists an increase in breakthrough time when bed depth of SBC@β-FeOOH varies from 0.7 to 1.5 cm at a flow rate of 1.0 mL min^{-1}, DC influent concentration of 27 mg L^{-1} and pH 6. The authors of this work calculated the empty bed contact time (EBCT) increasing from 0.198 to 0.424 min, as increasing the bed depth, it represents that DC molecules make an efficient diffusion into the porous structure present in SBC@β-FeOOH, it increases the bed-depth. Under this condition, the introduced mass-transfer zone moves further towards down, when increasing the bed depth, allows efficient contact between DC and SBC@β-FeOOH present in column. Beside of this, slope present in breakthrough curve tends to be reduced with increase in bed depth, represents broadening in mass transfer zone. Additionally, the authors of this work evaluated the influence of pH in absorption efficiency of DC and found that for lower pH, protonation from SBC@β-FeOOH tends to be increase and it results to an increase in active sites on adsorbent surface. Hence there exists an increase in diffusion rate of DC into porous architecture of sorbent. Thereby, adsorption capacity of DC tends to be increase in acidic condition which results from cationic character in DC. The authors of this work found that lower value of influent DC concentration, low flow rate and high bed height increase adsorption rate of DC in SBC@β-FeOOH column. To exemplify synergistic effect from adsorption and in heterogeneous Fenton reaction, the authors of this work regenerated the DC saturated beds through flowing an H_2O_2 aqueous solution. There exists a small change in regeneration efficiency hold by SBC@β-FeOOH beds, if it is regenerated using various H_2O_2 doses. Here the authors of this work calculated the regeneration efficiency for saturated SBC@β-FeOOH in H_2O_2 as 78.1%, 90.6%, 65.6%, and 56.3% in feed with concentration as 3%, 5%, 10%, and 15% (in wt%), respectively. Prominently, regeneration efficiency obtained for SBC@β-FeOOH catalyst was easily controlled with adjusting H_2O_2 dosage. For lower H_2O_2

Open Access Article. Published on 20 November 2025. Downloaded on 12/25/2025 12:38:03 AM.
This article is licensed under a Creative Commons Attribution-NonCommercial 3.0 Unported Licence.

RSC Sustainability Accepted Manuscript

View Article Online
DOI: 10.1039/D5SU00525F

dosage, here OH and OOH radicals are introduced by Fenton-like reaction, it attacks DC molecules in an easier way. But for high concentration of H_2O_2 like 10% and 15%, the radical species scavenging by H_2O_2 is more significant, thereby there exists a reduction in total degradation efficiency hold by DC. The proposed results show that flow in relatively low concentration by H_2O_2 aqueous effectively restore sorption capacity hold by resultant SBC@β-FeOOH composite. Here, regeneration efficiency obtained for SBC@β-FeOOH having 5% H_2O_2 shows a slight reduction in adsorption capacity while first and the second cycle of adsorption. This is introduced from efficient affinity of intermediate products introduced during degradation process delivered by DC. A pictorial representation of in-situ regeneration process delivered by resultant SBC@β-FeOOH composite is shown in **Fig. 7**.

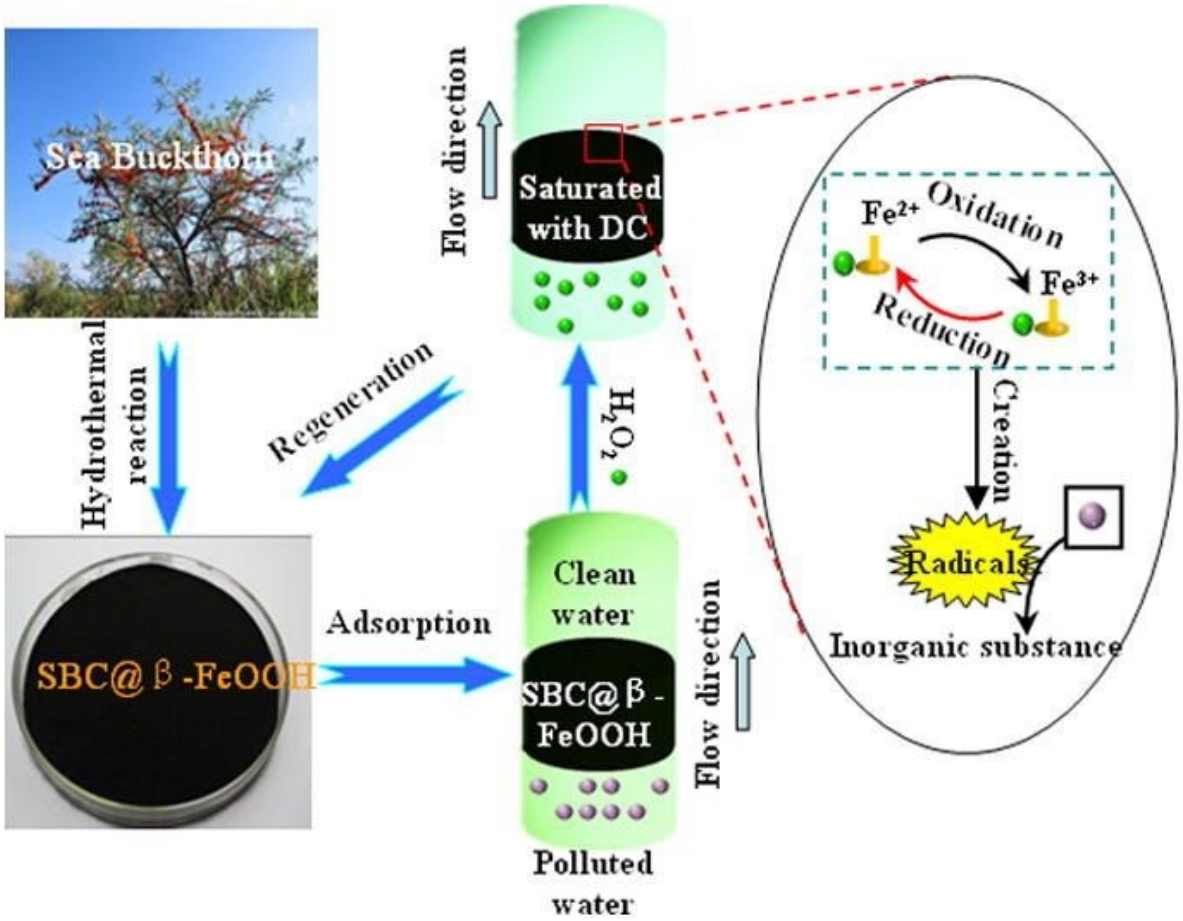

Open Access Article. Published on 20 November 2025. Downloaded on 12/25/2025 12:38:03 AM.
This article is licensed under a Creative Commons Attribution-NonCommercial 3.0 Unported Licence.

RSC Sustainability Accepted Manuscript

View Article Online
DOI: 10.1039/D5SU00525F

Fig. 7. Schematic representation of in-situ regeneration phenomena holds by β-FeOOH composite and its synergistic influence on removing aqueous DC solution. Reproduced with permission from [65] Copyright (2016) Elsevier Inc.

Open Access Article. Published on 20 November 2025. Downloaded on 12/25/2025 12:38:03 AM.
This article is licensed under a Creative Commons Attribution-NonCommercial 3.0 Unported Licence.

The regeneration phenomena are corresponding to synergistic phenomena; it works through the cooperation by SBC biosorption merits and catalytic heterogenous oxidation features from β-FeOOH nanoparticles. In a more specific way, DC molecules are tended to be transferred from aqueous solution to SBC through sorption and it pre-concentrated on bare areas present in SBC@β-FeOOH. Then, DC adsorbed molecules tend to be oxidized with β-FeOOH/ H_2O_2 heterogenous Fenton-like oxidation by a switching to H_2O_2 flow in water, it generated the radical species. Initially, SBC≡Fe^{3+} was reduced towards SBC≡Fe^{2+} through H_2O_2, which generates OOH radical. In the second step, the produced SBC≡Fe^{2+} reacts to another molecule in H_2O_2, which introduce hydroxyl anion and the OH radical. Additionally, H_2O_2/SBC≡Fe^{3+} introduced SBC≡Fe^{2+} and the OOH radical followed with SBC≡Fe^{2+} reoxidation through H_2O_2. Thus, DC molecules are tended to be oxidized through combined phenomena from OH and OOH radical and DC molecule adsorbed on hybrid nanocomposite was completely removed. Hence, saturated adsorption site on SBC@β-FeOOH nanocomposite surface was easily regenerated and it delivers the efficient capability of prepared composite for practical removal of adsorbents and organic compound destruction in wastewater. With the aid of efficient and new flow capacitive deionization (FCDI) approach, Li et al. [66] introduced a flowable electrode which introduce a biocarbon materials having fiber structured as a conductive agent in activated carbon (AC). Hence, it improves active substance utilization through conductive network introduced by fiber carbon materials. The authors of this work observed that AC with 5 wt% and carbonization bacterial cellulose having 0.25 wt% delivers a high salt ion adsorption capacity of 1.26–5.92 mM $m^{-2}s^{-1}$ and AC with 5 wt% possess 0.09–2.58 mM $m^{-2}s^{-1}$ under

RSC Sustainability Accepted Manuscript

View Article Online
DOI: 10.1039/D5SU00525F

Open Access Article. Published on 20 November 2025. Downloaded on 12/25/2025 12:38:03 AM.
This article is licensed under a Creative Commons Attribution-NonCommercial 3.0 Unported Licence.

saline condition at a potential of 1.8 V. Through physical and the electrochemical analysis, the authors of this work found that this cellulose has higher aspect ratio, as a conductive agent which is introduced through interconnected conductive network in more readily than carbonization chitin introduction having reduced adsorption rate, the untreated CNTs or carbon black spherical particle, thereby increasing total conductivity of electrode flow suspension. The AC synthesized in procedure of simultaneous pyrolysis and in activation of lemon balm and mint herbs utilized with H_3PO_4 was introduced for the purification of aqueous solution contain aresenate, cadmium poly(acrylic) acid and polyethylenimine. Here, the authors of this work observed that arsenate removal from aqueous solution is depends upon pH, but adsorption of cadmium on activated biocarbon surface is not depends upon their parameter. The maximum value of adsorption quantity to be calculated as 135.8 mg g^{-1} and 109.6 mg g^{-1} in the case of cadmium and arsenate respectively. The metal ions removal and polymers introduced from binary systems are found to lower value in compared with one-component solution. It is due to the result of polymer-metal complexes, that remains in solution [67]. Using CDI route, Zhang et al. [68] synthesized bio-carbon material which is nitrogen and phosphorous co-doped (N/P) with alkali lignin (AL) and the ammonium polyphosphate (APP) as carbon precursor based on a laser-induced carbonization (LIC) and a hydrothermal reaction strategy. A schematic representation of synthesis procedure is shown in **Fig. 8**.

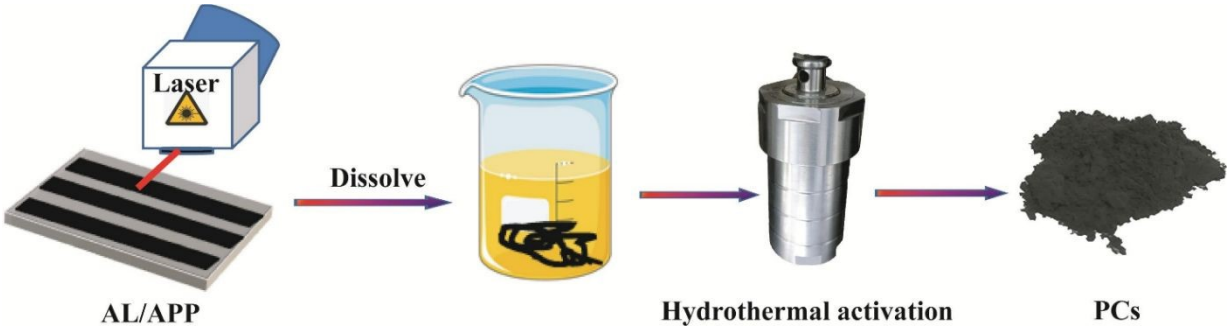

Fig. 8. Pictorial representation for synthesizing porous carbon material through LIC and hydrothermal strategy. Reproduced with permission from [68] Copyright (2024) Elsevier Inc.

RSC Sustainability Accepted Manuscript

View Article Online
DOI: 10.1039/D5SU00525F

The FESEM image for porous carbon synthesized is shown in **Fig. 9**. From **Fig. 9a-c**, it is clear that AL/APP hold foamlike architecture with exceptionally uneven distribution of pores and it macroporous are around 1 μm. AL makes a rapid decomposition and it release gas molecules under photothermal effect introduced by laser scanning, which leaves a porous architecture. At the same time, the literature shows that Al possesses high level of porosity after performing activation, where some of the decomposition APP products can't discharged efficiently in shorter duration of laser scanning. Here P_2O_5 blocks part of holes. As for LIC product introduced from AL, the proposed structure is observed to be prominently looser, having uniformity in distribution of porous architecture (**Fig. 9d** and **e**) and a prominent mesoporous architecture was observed in it (**Fig. 9f**). However, this obtained porous structure was consists of large quantity of nano-carbon particles, it is loose and easier to collapse under external force. This dramatic change in microstructure obtained between AL and AL/APP is through the photo-thermal effect from laser and efficient synergistic physio-chemical activation from APP. The AL/APP pore architecture was introduced by hydrothermal activation and microstructure of resultant H-AL/APP as shown in **Fig. 9g-i**. Distinctly, the hydrothermal activation provides higher amount of uniform pore architecture in H-AL/APP having porosity in down to the nanoscale (**Fig. 9g**). For high magnification, beehive like porous hierarchical architecture in H-AL/APP is observed.

Open Access Article. Published on 20 November 2025. Downloaded on 12/25/2025 12:38:03 AM.
This article is licensed under a Creative Commons Attribution-NonCommercial 3.0 Unported Licence.

RSC Sustainability Accepted Manuscript

rticle Online
SU00525F

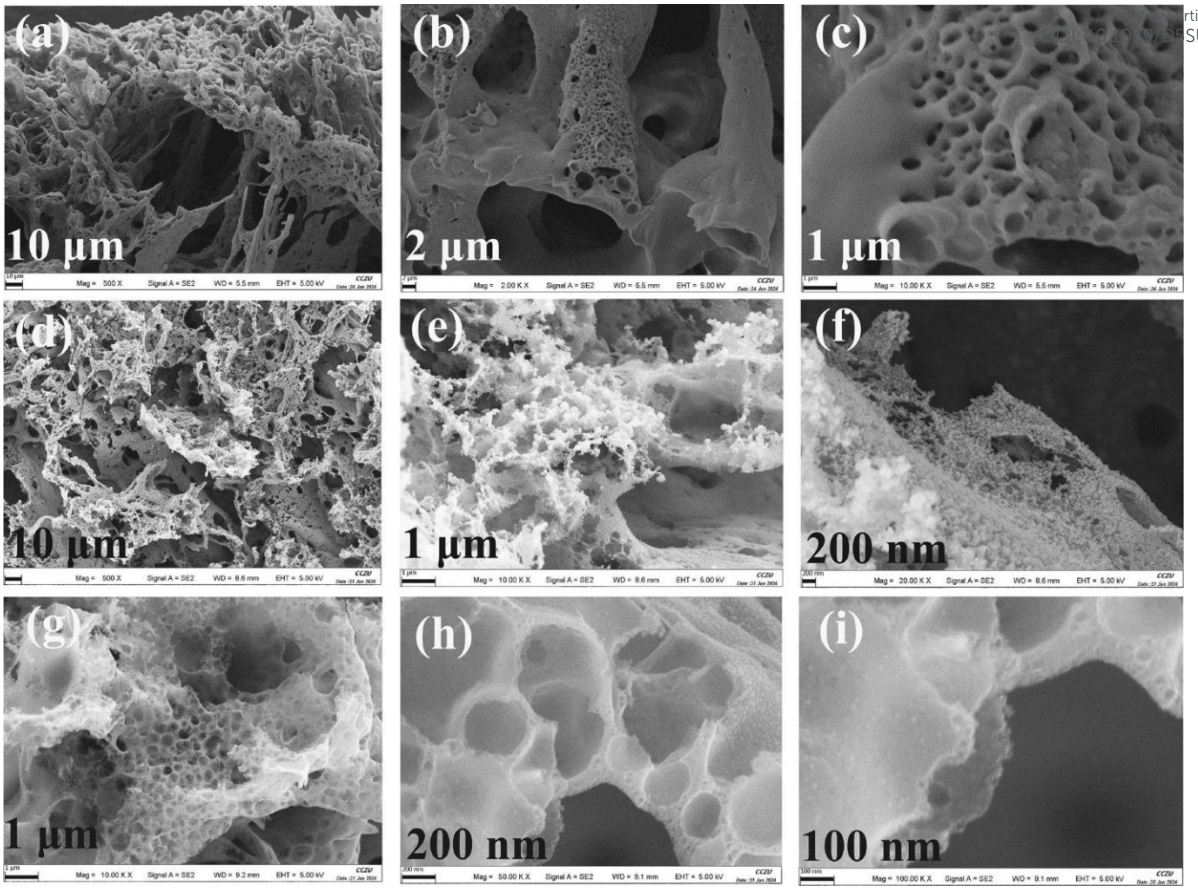

Fig. 9. SEM image for various magnifications corresponding to (a-c) AL/APP, (d-f) AL and (g-i) H-AL/APP. Reproduced with permission from [68] Copyright (2024) Elsevier Inc.

To compare desalination characteristics of CDI for H-AL/APP and YP80, the authors of this work performed experiment using 500 mg L^{-1} in NaCl solution upto conductivity tends to be stable for eliminating influence on physical adsorption on real-time electro-adsorption capacity. **Fig. 10a** represents curve corresponding to solution conductivity with respect to time while CDI experiment having two electrodes and both of it show similar trend in downward direction. In initial stage, electrode consists of large quantity of unoccupied active site, it facilitates adsorption of higher number of Na^+/Cl^- and faster formation of electrical double layer, which leads to sharp reduction in conductivity. Here reduction in conductivity gradually reduce with respect to time and then tends to be level off, it is due to the gradual approach of their adsorption capacity to limit value. During CDI process, conductivity value of solution

Open Access Article. Published on 20 November 2025. Downloaded on 12/25/2025 12:38:03 AM.
This article is licensed under a Creative Commons Attribution-NonCommercial 3.0 Unported Licence.

RSC Sustainability Accepted Manuscript

View Article Online
DOI: 10.1039/D5SU00525F

consists of H-AL/APP remains lowest, representing faster rate for electro-adsorption and large electro-adsorption capability. The adsorption capacity diagram is given in **Fig. 10b** and the H-AL/APP have highest adsorption capacity value of 34.7 mg g^{-1}, which is found to be 1.5 time greater than YP80. The authors of this work evaluated the adsorption kinetics of two electrodes further verified through CDI Ragone plot, as given in **Fig. 10c**. Prominently, the H-AL/APP data was located in upper right corner portion of YP80, it represents faster rate of adsorption under similar adsorption capacity. Additionally, the authors of this work performed test with 500 mg L^{-1} NaCl circulated for evaluating their stability character and reusability (**Fig. 10d**). In the procedure of five stages of CDI cycles, it maintains the lowest conductivity for solution and it maintained for a range of 1.15-1.20 mS cm^{-1}, represents higher cycle stability with regeneration performance capability. The proposed desalting capability and cyclic stability performance is through increase in defect structure present in carbon material and acquisition by higher number of active sites after doping with N/P, thereby improves its wettability and their conductivity. The presence of higher degree of favourable specific surface area with efficient layer for ion transfer provides desalination of CDI.

Open Access Article. Published on 20 November 2025. Downloaded on 12/25/2025 12:38:03 AM.
This article is licensed under a Creative Commons Attribution-NonCommercial 3.0 Unported Licence.

RSC Sustainability Accepted Manuscript

View Article Online
DOI: 10.1039/D5SU00525F

Open Access Article. Published on 20 November 2025. Downloaded on 12/25/2025 12:38:03 AM.
This article is licensed under a Creative Commons Attribution-NonCommercial 3.0 Unported Licence.

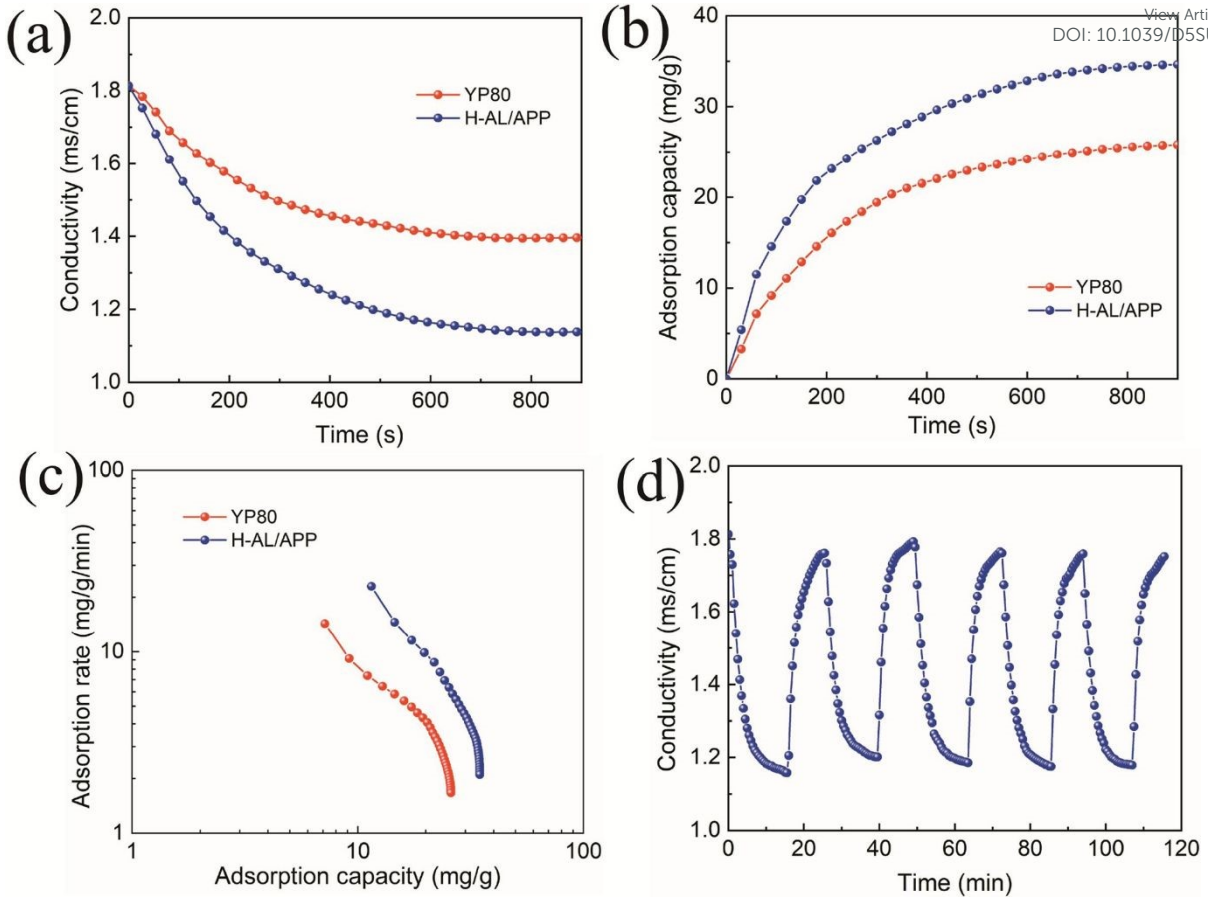

Fig. 10. (a) Variation curve for conductivity; (b) electro-adsorption capacity; (c) Ragone plot for YP80 and the H-CL/APP; (d) Measurement of cyclic capability for H-CL/APP. Reproduced with permission from [68] Copyright (2024) Elsevier Inc.

Ławi´nska et al.[69] utilized carbonization lime mud produced as a by-product of sugar production from purification of raw beetroot juice. In mean, while one campaign, the authors of this work obtained more than 12,000 ton of carbonization lime mud which allows it utilization as soil improver. Using chemical composition analysis, the authors of this work observed physical characteristics of waste and the authors performed all experiments in disc granulator. The authors of this work wetted this granulated material using water and an aqueous solution having molasses. The authors found that beds wetted using molasses of 33 and 66% solutions are characterized through higher homogeneity and a small size in resultant product. While experiments with wetting using water, the resultant product after performing drying

RSC Sustainability Accepted Manuscript

View Article Online
DOI: 10.1039/D5SU00525F

illustrated a reduced resistance for compression. On the otherhand, granules wetting by 33% aqueous solution illustrated resistance for compression, below a value of 10 N; and wetting granules wetting by aqueous solution of 66% molasses illustrated a resistance for compression above 10 N. Using a green technology, solar-driven water evaporation route with the aid of Co/CoO nanoparticle loaded by tobacco stem (TS) organisms, Liu et al.[70] synthesized TS-Co/CoO by one-step pyrolysis for waste-water purification. For the initial step of this work, the authors of this work utilized various routes for the synthesis of different biochar material for studying solar evaporation. Initially, the authors of this work used a magnifying glass for focussing sunlight on grapefruit skin for a duration of 5 s for generating carbon black grapefruit material (CPP (Sun)). In the same time, hydrothermal approach was introduced to reacting with pomelo peel at a temperature of 200ºC for a duration of 24 h and it is kept for freeze-drying for producing brown coloured pomelo peel carbon material (water heat). Additionally, the authors of this work synthesized black eucalyptus leaf material (EL) and TS through similar hydrothermal approach. The authors of this work evaluated the crystalline properties of prepared TS-Co/CoO (X) where X corresponding to impregnation $Co(NO_3)_2$ concentration values of 0.05, 0.10, 0.20 and 0.40 M. The authors observed an increase in impregnation concentration, where Co peak getting sharply, represents sample crystallization is better. The authors of this work evaluated the morphological characteristics of tobacco stem impregnated biocarbon with Co solution at various concentrations using SEM, as given in **Fig. 11.** It is found that morphological features hold by TS-Co/CoO(X) was consists of natural structure introduced from tobacco stem plants. Here material surface is observed to be rough after hydrolytic chemical changes from cobalt nitrate. Notably, the entire Co and CoO particle anchored on stem biocarbon surface represents efficient interaction present between Co, CoO and tobacco stem carbon carrier. The influence of impregnation concentration on morphological features of TS-Co/CoO(X) was evaluated. With respect to the increase in

Open Access Article. Published on 20 November 2025. Downloaded on 12/25/2025 12:38:03 AM.
This article is licensed under a Creative Commons Attribution-NonCommercial 3.0 Unported Licence.

RSC Sustainability Accepted Manuscript

View Article Online
DOI: 10.1039/D5SU00525F

impregnation concentration, the amount of Co and CoO particle on TS surface is tends to be increase prominently, but particle morphology is changed significantly. Here, the particle size of TS-Co/CoO(0.05) tends to be small and it distributed evenly (**Fig. 11a**), but XRD results indicates poor crystallinity at this time. From **Fig. 11b**, it is clear that the Co species loaded over TS-Co/CoO(0.10) shows irregular polyhedral architecture and it make an even distribution on tobacco stem carbon. As given in **Fig. 11c**, Co species part of TS-Co/CoO(0.20) changing from its polyhedron irregular structure to rod-like, with a reduction in particle size. Here, **Fig. 11d**, shows that when concentration of impregnation attains 0.40 M, the metal particle loaded over carbon carrier of tobacco stem shows serious agglomeration, indicates a higher concentration of impregnation. With the help of detailed morphological evaluation using TEM, the authors of this work found an even dispersion of Co/CoO nanoparticle on surface and in the matrix of tobacco stem biochar. Using size distribution diagram evaluation, the authors of this work obtained an average particle size of 33.26 nm in the case of Co/CoO nanoparticle. For making a systematic evaluation hot water photo evaporation characteristic, the authors of this work performed the experiment under simulated sunlight with an intensity of 1 sun. The authors of this work obtained an evaporation rate with photothermal conversion efficiency corresponding to TS-Co/CoO(0.20) as 2.22 kg m^2 h^{-1} and 13.94%, respectively.

Open Access Article. Published on 20 November 2025. Downloaded on 12/25/2025 12:38:03 AM.
This article is licensed under a Creative Commons Attribution-NonCommercial 3.0 Unported Licence.

RSC Sustainability Accepted Manuscript

Article Online
5SU00525F

Open Access Article. Published on 20 November 2025. Downloaded on 12/25/2025 12:38:03 AM.
This article is licensed under a Creative Commons Attribution-NonCommercial 3.0 Unported Licence.

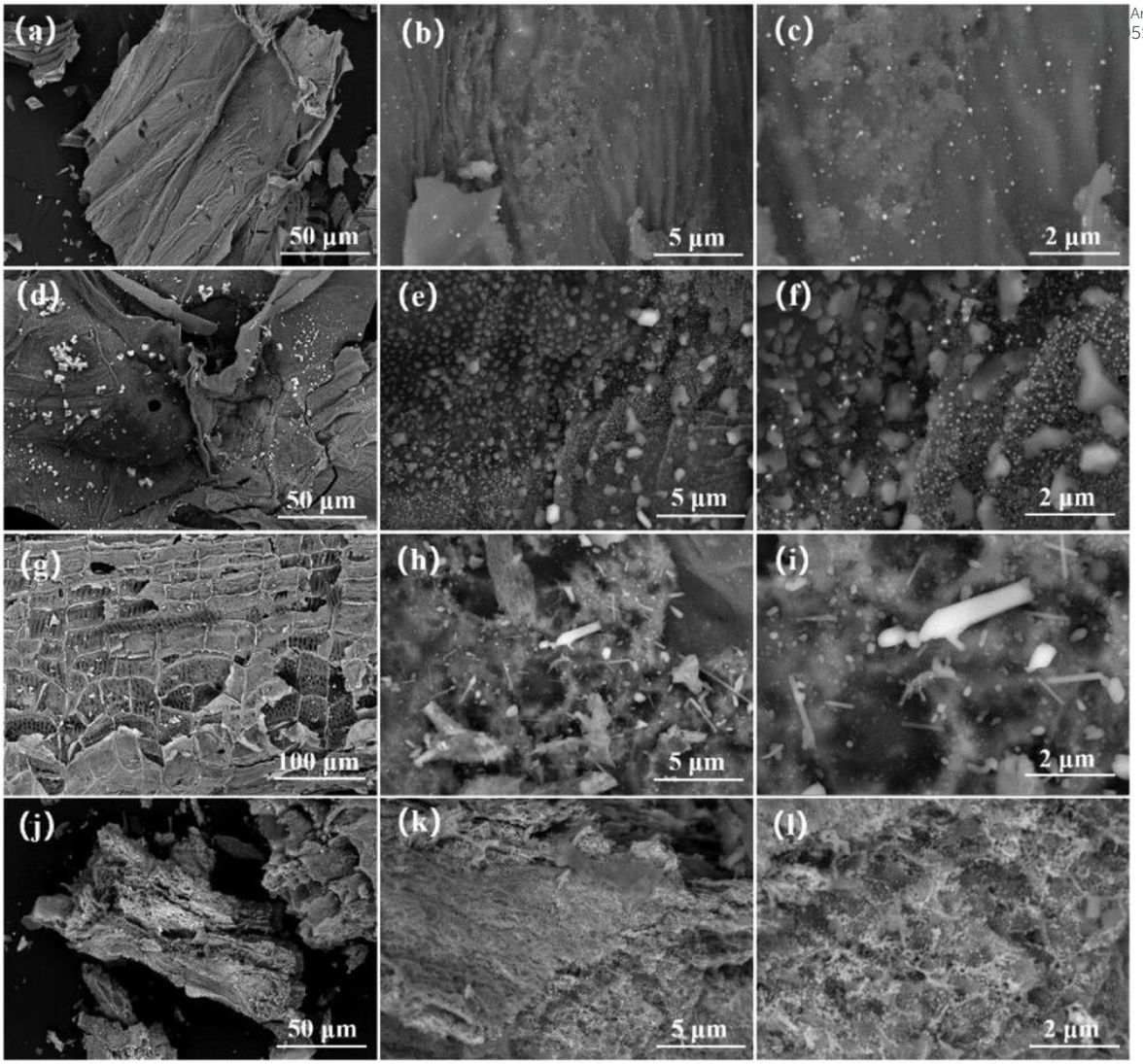

Fig. 11. SEM image for (a–c) TS-Co/CoO (0.05), (d–f) TS-Co/CoO (0.10), (g–i) TS-Co/CoO (0.20), and (j–l) TS-Co/CoO (0.40). Reproduced with permission from [70] Copyright (2024) Wiley-Verlag VCH Ltd.

This evaporation rate was observed to be about 1.47 times greater than TS-500 and 4.35 times greater than pure water. The evaporation rate of water is prominently better than TS-500 without applying any loading of Co/CoO nanoparticle. More than this, the prepared material exhibits an efficient water evaporate rate, it is better than most of the solar evaporation photothermal material having similar type. Here, synergistic influence from Co/CoO having carbon material will limit heat to evaporation surface, prominently reduce heat loss and

RSC Sustainability Accepted Manuscript

View Article Online
DOI:10.1039/D5SU00525F

Open Access Article. Published on 20 November 2025. Downloaded on 12/25/2025 12:38:03 AM.
This article is licensed under a Creative Commons Attribution-NonCommercial 3.0 Unported Licence.

relatively increase efficiency of evaporation. When intensity of light one the intensity of solar light, evaporation mass of water delivered by TS-Co/CoO(0.20) nanocomposite will reach 2.32 kg after inducing 1 h of light, it is greater than 0.51 kg mass loss under natural evaporation condition. When concentration of impregnation reaches 0.40 M, there exists a sharp reduction in evaporation rate and it is through the nanoparticle agglomeration at high impregnation concentration, thereby reduction in absorption capacity for light by the material. Additionally, the authors evaluated the material stability for practical application. After each cycle of the experiment, TS-Co/CoO(0.20) material tends to be naturally dried and it is recovered. The authors used TGA analysis for verifying thermal stability of material's water evaporation property. Using TGA analysis, the authors of this work observed a degradation at a temperature of 332ºC, it ensures structural stability at a normal value of operating temperature. To evaluate light absorption features of TS-Co/CoO(0.20) material, the authors of this work analysed infrared and the ultraviolet spectra for prepared samples. From this analysis, the authors of this work found that TS-Co/CoO(0.20) have better absorption characteristics than TS-500, it makes an expansion in an energy range that tends to be converted towards heat. It is through the multiple internal reflections present inside the Co/CoO dense nanoparticle layer in the TS-Co/CoO(0.20), thereby increase light reflection, indicates the tobacco stem carbonized support layer and the Co/CoO nanoparticle metal plasma absorbs double role of the sunlight, having broad absorption spectrum of light, which meets the requirement from efficient solar energy interface dilution. In the ultraviolet and in visible wavelength, reflectivity value of TS-Co/CoO(0.20) is smaller than TS-500 and TS-raw, indicates Co/CoO particle surface and the porous architecture in TS-Co/CoO(0.20) capture higher amount of incident light. Additionally, after loading Co/CoO nanoparticle, graphitization degree hold by TS-Co/CoO(0.20) material is increased, it is conductive for improving absorption capability of light in the material. For the solar desalination phenomena, hydrophilicity is a major criterion, and channels for

RSC Sustainability Accepted Manuscript

View Article Online
DOI: 10.1039/D5SU00525F

hydrophilic performance facilitates rapid supply of water for water evaporation. Using IR spectrum, the authors of this work observed two prominent characteristic peak presents at 3440 and 1630 cm^{-1} of two materials are corresponding to –OH and –COOH group stretching vibration, respectively, which confirms the presence of hydrophilic groups in it.

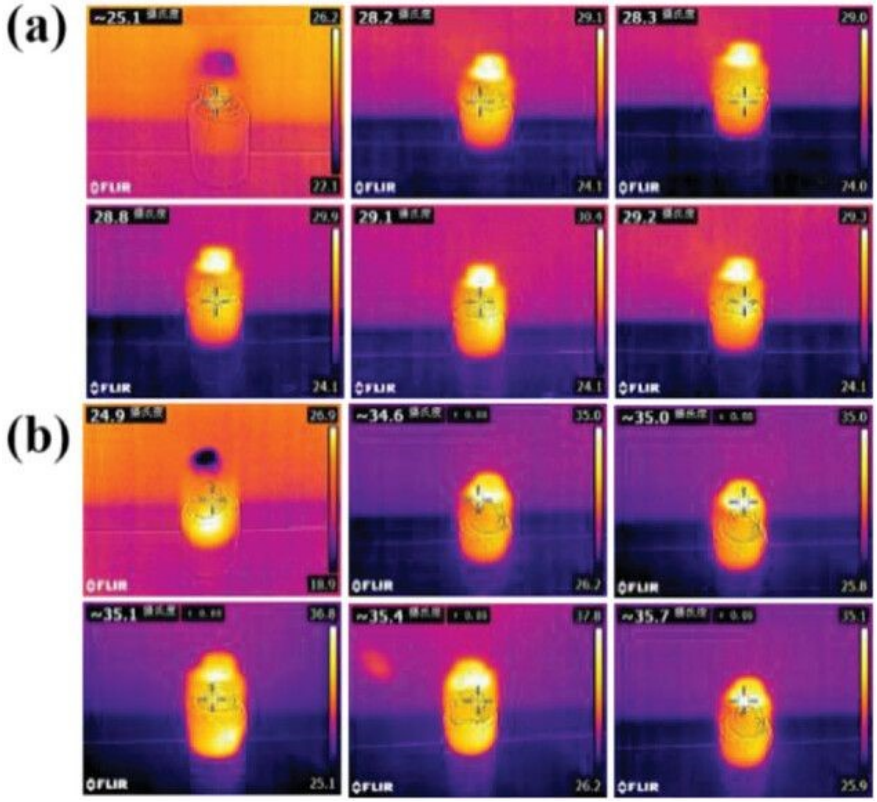

Fig. 12. (a) Changes in temperature for (a) pure water and in (b) TS-Co/CoO (0.20). Reproduced with permission from [70] Copyright (2024) Wiley-Verlag VCH Ltd.

To further evaluate hydrophilicity of material, the authors of this work have taken dynamic contact angle measurement and the obtained result shows that TS-Co/CoO(0.20) is highly hydrophilic than compared to TS-500 and water molecules make a rapid transport in material. Particularly, higher number of microscopic pores present in tobacco stem which is carbonized can utilize capillary water for flow into the hot region, thus water on surface of material can rapidly replenished after performing evaporation. For studying the photothermal conversion capability of material, for evaporation by water test, the authors of this work recorded

Open Access Article. Published on 20 November 2025. Downloaded on 12/25/2025 12:38:03 AM.
This article is licensed under a Creative Commons Attribution-NonCommercial 3.0 Unported Licence.

RSC Sustainability Accepted Manuscript

View Article Online
DOI: 10.1039/D5SU00525F

temperature change on surface of TS-Co/CoO(0.20) material before and after light in a duration of 0 to 75 min with thermal infrared imager. As given in **Fig. 12b**, surface temperature value of TS-Co/CoO(0.20) increases from a room temperature range to maximum value of 35.7ºC with illumination and this rise in temperature is stable with respect to time. This represents that synthesized TS-Co/CoO(0.20) material have efficient photothermal conversion capability, and it provides high temperature to heat thin form of water layer and improves their evaporation. After modifying the Co/CoO nanoparticle, surface hold by tobacco stem carbon material is observed to be rough, and rougher character of this surface is favourable for absorption of light, which makes a reduction in reflected energy loss, thus improves absorption of light in multiple internal reflection, and it effectively converts absorbed light to the heat. By using agricultural rice husk waste as biochar source and synthesized biochar-loaded nano zero-valent iron with high-temperature pyrolysis combined by carbothermal reduction [71]. Here iron compounds tend to be reduced towards valent non-zero iron and biomass tends to be turned to a biochar and the authors of this work used the resultant product (BC@nZVI) for activating sodium persulfate in order to remove rhodamine B (RhB) dye. Through SEM analysis, the authors of this work observed nZVI particle with amorphous character and it is dispersed on biochar surface. The loading of nZVI changes morphology and obtained structural features of biochar, which represents its excellent biochar dispersion, thereby maintains stability and nZVI dispersion and improves resistance for agglomeration and catalytic efficiency. The authors of this work observed that after loading nZVI on biochar surface which improves redox reaction between the Fe^{2+} and Fe^{3+} and promotes the $SO_4^{\bullet-}$ production and reduced pyrolysis temperature with higher Fe loading was determined for RhB removal. The authors of this work found that the dosage of BC@nZVI, presence of inorganic anion, the initial value of pH and various temperature hold various degree of influence on removal of RhB. Here the authors found that low value of pH and a higher temperature hold beneficial characteristics for RhB removal. For

Open Access Article. Published on 20 November 2025. Downloaded on 12/25/2025 12:38:03 AM.
This article is licensed under a Creative Commons Attribution-NonCommercial 3.0 Unported Licence.

RSC Sustainability Accepted Manuscript

View Article Online
DOI: 10.1039/D5SU00525F

Open Access Article. Published on 20 November 2025. Downloaded on 12/25/2025 12:38:03 AM.
This article is licensed under a Creative Commons Attribution-NonCommercial 3.0 Unported Licence.

neutral value of pH (6±2) and at a room temperature value of 25ºC, the authors of this work obtained a removal efficiency for RhB as 90.1% in 120 min. The obtained results show that $\bullet SO_4^-$ and the •OH plays beneficial effect on the proposed system, but $\bullet SO_4^-$ as dominant species. There is a work which aims to characterize adsorptive features of activated charcoal based on pharmaceutical (biocarbon and the Dyna) for adsorption of the reactive orange 16 (RO16) and the RhB [72]. The authors of this work utilized commercially activated carbon for its comparison. The authors evaluated the textural features and its functional groups. In the FTIR spectra the authors of this work found that there exist a broad and strong band at the wavenumber range of 3600-3100 cm^{-1} which is assigned to the stretching vibration from -OH group. In the case of commercially available carbon, the band present at the wavenumber range 3600-3200 cm^{-1} is the moisture content, it is evident from the two peaks present at 4000-3600 cm^{-1}. Here intensity of peak is reduced in the order of Dyna>biocarbon>commercially available carbon. In FTIR, the peak exists at 3000-2850 cm^{-1} shows existence of alkyl group, the vibration of $-CH_2$, here Dyna possesses high intensity when compared with biocarbon. The alkene group attributes to broader peak for a wavenumber of 1680-1600 cm^{-1} in the case of activated charcoals and in commercially available carbon, but the symmetric C=C aromatic stretch present at the wavenumber of 1600-1500 cm^{-1} is exclusive in commercially available carbon which signifying the evolution of graphitic architecture. Here peak for 1470–1350 cm^{-1} represent bending vibration of CH_2, but the high intense peak for 1200–900 cm^{-1} is by the stretching vibration of –CO. From the surface area analysis, the authors found that the specific surface is in the order of commercially available carbon>biocarbon>Dyna. The commercially available carbon hold surface area value of 909 $m^2\ g^{-1}$ and removal efficiency of 69.4 mg g^{-1} in the case of RO16. But for biocarbon it holds a higher removal efficiency for RhB as 54.5 mg g^{-1}, with a low surface area value of 172 $m^2\ g^{-1}$. From this evaluation, the authors observed that pharmaceutical related activated charcoal is a prominent adsorption candidate in the dye-

RSC Sustainability Accepted Manuscript

View Article Online
DOI: 10.1039/D5SU00525F

laden treatment of wastewater. A biodegradable and recyclable ligano-cellulosic banana fibers are synthesized from banana plant's perennial herb[73]. These fibers are used for removing anionic dyes such as alizarin red S, crystal violet, methyl violet and methyl orange from water. The authors synthesized this banana fibers using carbonization procedure of banana raw fibers. The authors of this work observed a tube-like architecture for these prepared fibers having diameter of this porous structure varies from 1.88 to 12.08 μm. Due to the availability of these efficient fibers with higher number of active sites provides efficient removal of this toxic dyes. The authors of this work obtained adsorption capacity values of 85.65, 78.95, 65.78 and 65.07 mg^{-1} in the case of methyl violet, methyl orange, crystal violet and alizarin red S, respectively. Hence, the authors of this work found that prepared sustainable banana fiber act as an efficient dye adsorbent for practical application.

3. Challenges and Future Perspectives

The present review depicts the features of biocarbon based materials for wastewater purification. It is found that the biocarbon feasibility on higher scale hinges not only in their technological characteristics, but also on economic viability and in environmental impact for production costs. An in-depth understanding on challenges and future perspectives related to this biocarbon based materials are necessary for implementing it in a wide platform. A schematic representation of challenges associated with the biocarbon based materials are shown in **Fig. 13**.

- The utilization of resources in nature which are compatible for act as a biocarbon is stand as a challenge. Thus, it is necessary to incorporate more material candidates available in nature for the extraction of biocarbon from it.
- Another drawback introduced for the utilization of biocarbon materials is the proper synthesis/extraction routes, which provides a bulk scale of production in a low-cost

Open Access Article. Published on 20 November 2025. Downloaded on 12/25/2025 12:38:03 AM.
This article is licensed under a Creative Commons Attribution-NonCommercial 3.0 Unported Licence.

RSC Sustainability Accepted Manuscript

View Article Online
DOI: 10.1039/D5SU00525F

way. The synthesis methods which are already established have problems relating the quantity of resultant product, a small scale of products is introduced from these routes, which is not to be compatible with the practical bulk scale water purification.

- A feasible risk analysis with sensitivity studies is necessary for the identification of parameters which are crucial for making environmental viability. In the bulk scale, the price for the biocarbon materials is in a wide range, the minimum value of selling price is a crucial fact, which makes the laboratory scale synthesis of these materials with the utilization of only available methods like pyrolysis, hydrothermal, etc.
- The deposition and the data sharing corresponding to biocarbon characteristics and its process conditions are crucial and it help for overcoming its issues relating to reproducibility, which provides useful information for connecting feedstocks, for process condition and the biocarbon features, which helps researchers and the industrial actors for make a better design to production protocols which is adapted for specific biocarbon quality. The correlation between extensive databases to connecting biocarbon features and its production routes from various resources are crucial for addressing reproducibility.
- Another difficulty in the field of biocarbon based materials is their development in large scale, such as scales required by different mitigation climate change scenarios, which produce adverse effect on natural ecosystem or food security through expansion in dedicated biomass plantation for the biochar feedstock at the expenses of forests or croplands.
- Through the cost-effective addition of binder or other feasible materials as a reinforcing candidate, we can able to tune the properties of biocarbon based materials in order to compete with the requirement of high-performing waste-water purification approach. Negotiations are important if carbon architecture and their architecture induced features

Open Access Article. Published on 20 November 2025. Downloaded on 12/25/2025 12:38:03 AM.
This article is licensed under a Creative Commons Attribution-NonCommercial 3.0 Unported Licence.

RSC Sustainability Accepted Manuscript

View Article Online
DOI: 10.1039/D5SU00525F

are tends to be unique and it prominently depends upon uniformity of source as hydrocarbons and its molecular freedom is through liquid/gas in feedstock.

- Additionally, the graphitized biocarbon material delivers a prominent technological advancement in order to meet the requirement of industrial applications. It is possible to establish a graphitized form of biocarbon through proper synthesis strategy.

By considering these facts and by finding suitable routes for synthesize, it is possible to optimize the physiochemical properties of biocarbon based materials. Thereby, we can use this sustainable, biodegradable biocarbon materials as a novel candidate for wastewater purification, in order to remove the current wastewater pollution and to avoid the scarcity of pure water requirement for contributing UN SDGs.

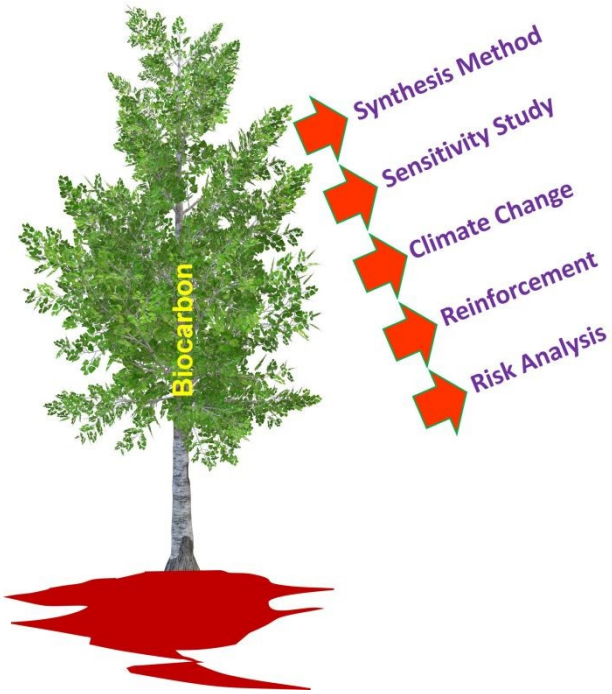

Fig. 13. Schematic representation of challenges associated with the biocarbon based materials.

4. Conclusions

Biocarbon based materials received tremendous attention as a futuristic source for waste water purification. From the present review, we found that the extraordinary physical and chemical

Open Access Article. Published on 20 November 2025. Downloaded on 12/25/2025 12:38:03 AM.
This article is licensed under a Creative Commons Attribution-NonCommercial 3.0 Unported Licence.

RSC Sustainability Accepted Manuscript

View Article Online
DOI: 10.1039/D5SU00525F

properties hold by the biocarbon based materials are meet the requirements of an excellent candidate for purifying wastewater. This not only compete with the current demand of freshwater requirement but also envisages an eco-friendly system for human beings and other living organisms. It is clear that biocarbon-based materials are capable to revolutionize wastewater treatment through facilitating an efficient, cost-efficient and sustainable solution for current challenges in environmental protection. The present review depicts that through the optimization of suitable synthesis approach we can able to modulate the physiochemical properties hold by biocarbon material for utilizing it as a catalytic substance in waste water purification. Through the review, we found that there is only limited number of publications based on the application of biocarbon based materials for waste water purification, more specifically we can say that it is still on their infancy stage. The review gives an outline that by focussing on proper synthesis method by extracting from natural products, it is possible to optimize the parameters which influencing the features of biocarbon materials for make it as global candidate for futuristic applications. By refining synthesis approaches, enhanced durability, estimating emerging contaminants and development of an integrated treatment system will facilitates suitable choice for wastewater purification. In this context, environment-friendly biocarbon are cost-effective materials simultaneously contribute to the SDGs goals and helps in circular economy.

References

[1] S.A. Thomas, J. Cherusseri, D.N. Rajendran, Loofah sponge: a sustainable material for wastewater desalination, RSC Sustainability, 3(2025)2806-2832.

[2] T. Hák, S. Janoušková, B. Moldan, Sustainable Development Goals: A need for relevant indicators, Ecological indicators, 60 (2016) 565-573.

Open Access Article. Published on 20 November 2025. Downloaded on 12/25/2025 12:38:03 AM.
This article is licensed under a Creative Commons Attribution-NonCommercial 3.0 Unported Licence.

RSC Sustainability Accepted Manuscript

View Article Online
DOI: 10.1039/D5SU00525F

[3] S.A. Thomas, J. Cherusseri, D.N. Rajendran, A Minireview on Rubber Nanocomposites for Sustainable Supercapacitors, RSC Sustainability, 3(2025)3358-3383.

[4] G. Assembly, Sustainable development goals, SDGs transform our world, 2030 (2015).

[5] M. Stafford-Smith, D. Griggs, O. Gaffney, F. Ullah, B. Reyers, N. Kanie, B. Stigson, P. Shrivastava, M. Leach, D. O'Connell, Integration: the key to implementing the Sustainable Development Goals, Sustainability science, 12 (2017) 911-919.

[6] A. Fleming, R.M. Wise, H. Hansen, L. Sams, The sustainable development goals: A case study, Marine Policy, 86 (2017) 94-103.

[7] D. Jaspal, A. Malviya, Composites for wastewater purification: A review, Chemosphere, 246 (2020) 125788.

[8] M. Yadav, R. Gupta, R.K. Sharma, Green and sustainable pathways for wastewater purification, In Advances in water purification techniques, Elsevier (2019), pp. 355-383.

[9] E. Iakovleva, M. Sillanpää, The use of low-cost adsorbents for wastewater purification in mining industries, Environmental Science and Pollution Research, 20 (2013) 7878-7899.

[10] Y. Shen, J. Tang, Z. Nie, Y. Wang, Y. Ren, L. Zuo, Preparation and application of magnetic Fe3O4 nanoparticles for wastewater purification, Separation and purification technology, 68 (2009) 312-319.

[11] N.A. Abd El-Ghany, M.H.A. Elella, H.M. Abdallah, M.S. Mostafa, M. Samy, Recent advances in various starch formulation for wastewater purification via adsorption technique: a review, Journal of Polymers and the Environment, 31 (2023) 2792-2825.

[12] N. Li, S. Wu, H. Dai, Z. Cheng, W. Peng, B. Yan, G. Chen, S. Wang, X. Duan, Thermal activation of persulfates for organic wastewater purification: Heating modes, mechanism and influencing factors, Chemical Engineering Journal, 450 (2022) 137976.

[13] J. Cherusseri, C.M. Savio, M. Khalid, V. Chaudhary, A. Numan, S.J. Varma, A. Menon, A. Kaushik, SARS-CoV-2-on-chip for long COVID management, Biosensors, 12 (2022) 890.

Open Access Article. Published on 20 November 2025. Downloaded on 12/25/2025 12:38:03 AM.
This article is licensed under a Creative Commons Attribution-NonCommercial 3.0 Unported Licence.

RSC Sustainability Accepted Manuscript

View Article Online
DOI: 10.1039/D5SU00525F

[14] M. Kitajima, W. Ahmed, K. Bibby, A. Carducci, C.P. Gerba, K.A. Hamilton, E. Haramoto, J.B. Rose, SARS-CoV-2 in wastewater: State of the knowledge and research needs, Science of the total environment, 739 (2020) 139076.

[15] H.N. Tran, G.T. Le, D.T. Nguyen, R.-S. Juang, J. Rinklebe, A. Bhatnagar, E.C. Lima, H.M. Iqbal, A.K. Sarmah, H.-P. Chao, SARS-CoV-2 coronavirus in water and wastewater: A critical review about presence and concern, Environmental research, 193 (2021) 110265.

[16] J. Peccia, A. Zulli, D.E. Brackney, N.D. Grubaugh, E.H. Kaplan, A. Casanovas-Massana, A.I. Ko, A.A. Malik, D. Wang, M. Wang, Measurement of SARS-CoV-2 RNA in wastewater tracks community infection dynamics, Nature biotechnology, 38 (2020) 1164-1167.

[17] A. Bivins, J. Greaves, R. Fischer, K.C. Yinda, W. Ahmed, M. Kitajima, V.J. Munster, K. Bibby, Persistence of SARS-CoV-2 in water and wastewater, Environmental Science & Technology Letters, 7 (2020) 937-942.

[18] A. Giacobbo, M.A.S. Rodrigues, J.Z. Ferreira, A.M. Bernardes, M.N. de Pinho, A critical review on SARS-CoV-2 infectivity in water and wastewater. What do we know?, Science of the Total Environment, 774 (2021) 145721.

[19] A. Zakari, I. Khan, D. Tan, R. Alvarado, V. Dagar, Energy efficiency and sustainable development goals (SDGs), Energy, 239 (2022) 122365.

[20] G. Crini, E. Lichtfouse, Advantages and disadvantages of techniques used for wastewater treatment, Environmental chemistry letters, 17 (2019) 145-155.

[21] G. Crini, E. Lichtfouse, Wastewater treatment: an overview, In Green adsorbents for pollutant removal: fundamentals and design, (2018) 1-21.

[22] D.H. Liu, B.G. Lipták, Wastewater treatment, CRC Press2020.

[23] P. Chowdhary, A. Raj, R.N. Bharagava, Environmental pollution and health hazards from distillery wastewater and treatment approaches to combat the environmental threats: a review, Chemosphere, 194 (2018) 229-246.

Open Access Article. Published on 20 November 2025. Downloaded on 12/25/2025 12:38:03 AM.
This article is licensed under a Creative Commons Attribution-NonCommercial 3.0 Unported Licence.

RSC Sustainability Accepted Manuscript

View Article Online
DOI: 10.1039/D5SU00525F

[24] J. Dhote, S. Ingole, A. Chavhan, Review on wastewater treatment technologies, Int. J. Eng. Res. Technol, 1 (2012) 01-10.

[25] R. Parra-Saldivar, M. Bilal, H.M. Iqbal, Life cycle assessment in wastewater treatment technology, Current Opinion in Environmental Science & Health, 13 (2020) 80-84.

[26] A.P. Machado, L. Urbano, A. Brito, P. Janknecht, J. Salas, R. Nogueira, Life cycle assessment of wastewater treatment options for small and decentralized communities, Water Science and Technology, 56 (2007) 15-22.

[27] C.E. Boyd, Water quality: an introduction, Springer Science & Business Media, (2000).

[28] R.D. Gupta, Environment Pollution: Hazards and Control, Concept publishing company, (2006).

[29] R. Burkhard, A. Deletic, A. Craig, Techniques for water and wastewater management: a review of techniques and their integration in planning, Urban water, 2 (2000) 197-221.

[30] Y. Ye, H.H. Ngo, W. Guo, Y. Liu, S.W. Chang, D.D. Nguyen, H. Liang, J. Wang, A critical review on ammonium recovery from wastewater for sustainable wastewater management, Bioresource Technology, 268 (2018) 749-758.

[31] K. Jain, A.S. Patel, V.P. Pardhi, S.J.S. Flora, Nanotechnology in wastewater management: a new paradigm towards wastewater treatment, Molecules, 26 (2021) 1797.

[32] S. Gupta, Y. Mittal, R. Panja, K.B. Prajapati, A.K. Yadav, Conventional wastewater treatment technologies, In Current developments in biotechnology and bioengineering, (2021) 47-75.

[33] G. Gedda, K. Balakrishnan, R.U. Devi, K.J. Shah, V. Gandhi, V. Gandh, K. Shah, Introduction to conventional wastewater treatment technologies: limitations and recent advances, Mater. Res. Found, 91 (2021) 1-36.

Open Access Article. Published on 20 November 2025. Downloaded on 12/25/2025 12:38:03 AM.
This article is licensed under a Creative Commons Attribution-NonCommercial 3.0 Unported Licence.

RSC Sustainability Accepted Manuscript

View Article Online
DOI: 10.1039/D5SU00525F

[34] D. Paredes, P. Kuschk, T. Mbwette, F. Stange, R. Müller, H. Köser, New aspects of microbial nitrogen transformations in the context of wastewater treatment–a review, Engineering in Life Sciences, 7 (2007) 13-25.

[35] M. van Afferden, J.A. Cardona, M.-Y. Lee, A. Subah, R.A. Müller, A new approach to implementing decentralized wastewater treatment concepts, Water Science and Technology, 72 (2015) 1923-1930.

[36] A. Raza, S. Altaf, S. Ali, M. Ikram, G. Li, Recent advances in carbonaceous sustainable nanomaterials for wastewater treatments, Sustainable Materials and Technologies, 32 (2022) e00406.

[37] S. Shan, Y. Zhao, H. Tang, F. Cui, A mini-review of carbonaceous nanomaterials for removal of contaminants from wastewater, IOP Conference Series: earth and environmental science, IOP Publishing, 2017, pp. 012003.

[38] Q. Zou, B. Wang, B. Gao, T. Jiang, Q. Feng, M. Chen, J. Zhang, X. Zhang, Roles and mechanisms of carbonaceous materials in advanced oxidation coupling processes for degradation organic pollutants in wastewater: a review, Biochar, 5 (2023) 86.

[39] A.K. Mohanty, S. Vivekanandhan, O. Das, L.M. Romero Millán, N.B. Klinghoffer, A. Nzihou, M. Misra, Biocarbon materials, Nature Reviews Methods Primers, 4 (2024) 19.

[40] M. Pahnila, A. Koskela, P. Sulasalmi, T. Fabritius, A review of pyrolysis technologies and the effect of process parameters on biocarbon properties, Energies, 16 (2023) 6936.

[41] M. Zaed, R. Saidur, A. Pandey, M. Kadhom, K. Tan, J. Cherusseri, N. Abdullah, Utilization of recycled materials for low-cost MXene synthesis and fabrication of graphite/MXene composite for enhanced water desalination performance, Separation and Purification Technology, 354 (2025) 129055.

Open Access Article. Published on 20 November 2025. Downloaded on 12/25/2025 12:38:03 AM.
This article is licensed under a Creative Commons Attribution-NonCommercial 3.0 Unported Licence.

RSC Sustainability Accepted Manuscript

View Article Online
DOI: 10.1039/D5SU00525F

[42] R.K. Mishra, M. Misra, A.K. Mohanty, Value-added bio-carbon production through the slow pyrolysis of waste bio-oil: fundamental studies on their structure–property–processing co-relation, ACS omega, 7 (2022) 1612-1627.

[43] M. Zaed, R. Saidur, A. Saleque, K. Tan, J. Cherusseri, A. Pandey, M. Kabir, Unlocking desalination's potential: Harnessing MXene composite for sustainable desalination, Chemical Engineering Journal, 500(2024) 156910.

[44] E. Behazin, M. Misra, A.K. Mohanty, Sustainable biocarbon from pyrolyzed perennial grasses and their effects on impact modified polypropylene biocomposites, Composites Part B: Engineering, 118 (2017) 116-124.

[45] L. Wang, Ø. Skreiberg, N. Smith-Hanssen, S. Jayakumari, S. Rørvik, G. Jahrsengene, S. Turn, Investigation of gasification reactivity and properties of biocarbon at high temperature in a mixture of CO/CO2, Fuel, 346 (2023) 128233.

[46] M. Zhou, Q. Wang, Y. Yuan, S.-H. Luo, Y.-H. Zhang, X. Liu, Biocarbon with different microstructures derived from corn husks and their potassium storage properties, Rare Metals, 40 (2021) 3166-3174.

[47] M. Yu, T. Saunders, T. Su, F. Gucci, M.J. Reece, Effect of heat treatment on the properties of wood-derived biocarbon structures, Materials, 11 (2018) 1588.

[48] M. Zaed, J. Cherusseri, R. Saidur, K. Tan, A. Pandey, Synthesis and characterization of hierarchical Ti3C2Tx MXene/graphitic-carbon nitride/activated carbon@ luffa sponge composite for enhanced water desalination, Open Ceramics, 19 (2024) 100645.

[49] S.A. Thomas, J. Cherusseri, D. N. Rajendran, R. Isaac, Functionalized Carbon Nanostructures for Wastewater Treatments, in: A. Barhoum, K. Deshmukh (Eds.) Handbook of Functionalized Carbon Nanostructures: From Synthesis Methods to Applications, Springer International Publishing, Cham, 2024, pp. 1971-2014.

Open Access Article. Published on 20 November 2025. Downloaded on 12/25/2025 12:38:03 AM.
This article is licensed under a Creative Commons Attribution-NonCommercial 3.0 Unported Licence.

RSC Sustainability Accepted Manuscript

View Article Online
DOI: 10.1039/D5SU00525F

[50] M. Zaed, J. Cherusseri, K. Tan, R. Saidur, A. Pandey, Hierarchical Ti3C2Tx MXene@ Honeycomb nanocomposite with high energy efficiency for solar water desalination, Chemosphere, 366 (2024) 143459.

[51] E. Weidner, E. Karbassiyazdi, A. Altaee, T. Jesionowski, F. Ciesielczyk, Hybrid Metal Oxide/Biochar Materials for Wastewater Treatment Technology: A Review, ACS Omega, 7 (2022) 27062-27078.

[52] A. Yadav, R. Dhankhar, Application of Metal Oxide Nanoparticles for Waste Water Treatment, in: N. Agarwal, M.P. Shah, V.S. Solanki, N. Singh (Eds.) Nanomaterials in Wastewater Research: Progress and Challenges, Springer Nature Singapore, Singapore, 2025, pp. 285-304.

[53] S.A. Thomas, J. Cherusseri, D.N. Rajendran, Strategically-designed hierarchical polypyrrole-modified manganese-doped tin disulfide (SnS2) nanocomposite electrodes for supercapatteries with high specific capacity, Electrochimica Acta, 504 (2024) 144910.

[54] S.A. Thomas, J. Cherusseri, D.N. Rajendran, Hierarchical two-dimensional layered nickel disulfide (NiS2)@ PEDOT: PSS nanocomposites as battery-type electrodes for battery-type supercapacitors with high energy density, Electrochem, 5 (2024) 298-313.

[55] S.A. Thomas, J. Cherusseri, D.N. Rajendran, R. Saidur, Graphitic Carbon Nitride and Their Derivatives, Handbook of Functionalized Carbon Nanostructures: From Synthesis Methods to Applications, Springer 2024, pp. 1-38.

[56] S.A. Thomas, J. Cherusseri, M.R. Pallavolu, D. N. Rajendran, D. Kumar, Boron Carbon Nitride (BCN): An Emerging Two-Dimensional Material for Rechargeable Batteries, Energy & Fuels, 38(2024)13704-13721.

[57] M. Singanan, E. Peters, Removal of toxic heavy metals from synthetic wastewater using a novel biocarbon technology, Journal of Environmental Chemical Engineering, 1 (2013) 884-890.

Open Access Article. Published on 20 November 2025. Downloaded on 12/25/2025 12:38:03 AM.
This article is licensed under a Creative Commons Attribution-NonCommercial 3.0 Unported Licence.

RSC Sustainability Accepted Manuscript

View Article Online
DOI: 10.1039/D5SU00525F

[58] S. Yeasmin, S. Bose, Carbon Based Polymer Composites in Water Treatment and Filtration, Biocarbon Polymer Composites, Bentham Science Publishers 2023, pp. 141-149.

[59] H. Hassen, Z. Yusuf, J. Sasikumar, Biocarbon derived from Lantana camara L. leaf and seed for adsorption of heavy metals from floriculture wastewater, Discover Environment, 3 (2025) 1-19.

[60] K. Sheoran, H. Kaur, S.S. Siwal, A.K. Saini, D.-V.N. Vo, V.K. Thakur, Recent advances of carbon-based nanomaterials (CBNMs) for wastewater treatment: Synthesis and application, Chemosphere, 299 (2022) 134364.

[61] B.S. Al-Anzi, O.C. Siang, Recent developments of carbon based nanomaterials and membranes for oily wastewater treatment, RSC advances, 7 (2017) 20981-20994.

[62] Z. Li, M. Wang, L. Chen, H. Ji, H.-Y. Yu, Highly efficient carbonization of nanocellulose to biocarbon aerogels with ultrahigh light absorption efficiency and evaporation rate as bifunctional solar/electric driven steam generator for water purification, Sustainable Materials and Technologies, 36 (2023) e00649.

[63] M. Zouari, L. Marrot, D.B. DeVallance, Evaluation of properties and formaldehyde removal efficiency of biocarbon prepared at variable pyrolytic temperatures, Frontiers in Environmental Science, 11 (2023) 1252926.

[64] V. Kannadhasan, K. Mahendran, R. Indhu, G. Manikannan, Strategic design of nitrogen and sulphur co-doped biocarbon/nickel hexacyanoferrate nanocomposite for efficient removal of ciprofloxacin and amoxicillin antibiotics from water, Diamond and Related Materials, 156(2025) 112420.

[65] X. Zhang, B. Bai, G.L. Puma, H. Wang, Y. Suo, Novel sea buckthorn biocarbon SBC@ β-FeOOH composites: efficient removal of doxycycline in aqueous solution in a fixed-bed through synergistic adsorption and heterogeneous Fenton-like reaction, Chemical Engineering Journal, 284 (2016) 698-707.

Open Access Article. Published on 20 November 2025. Downloaded on 12/25/2025 12:38:03 AM.
This article is licensed under a Creative Commons Attribution-NonCommercial 3.0 Unported Licence.

RSC Sustainability Accepted Manuscript

View Article Online
DOI: 10.1039/D5SU00525F

[66] D. Li, H.-n. Huang, X. Yang, Y. Yang, S. Bian, F. Li, H. Fang, C. Yu, F. Lai, Acid-free treatment of fiber-structured biocarbon material enhances flow capacitive deionization performance, Separation and Purification Technology, 330 (2024) 125288.

[67] M. Gęca, M. Wiśniewska, P. Nowicki, G. Wójcik, Arsenate and cadmium ions removal from multicomponent solutions of ionic polymers using mesoporous activated biocarbons, Journal of Molecular Liquids, 407 (2024) 125270.

[68] X. Zhang, H. Yang, S. Liu, J. Li, Laser-induced nitrogen and phosphorus-doped spongy carbon with graphene wings derived from lignin for significantly enhanced capacitance deionization performance, Separation and Purification Technology, 351 (2024) 128072.

[69] K. Ławińska, S. Szufa, A. Obraniak, T. Olejnik, R. Siuda, J. Kwiatek, D. Ogrodowczyk, Disc granulation process of carbonation lime mud as a method of post-production waste management, Energies, 13 (2020) 3419.

[70] Y. Liu, C. Zhang, A. Zhang, J. Zhang, L. Zhang, M. Huang, J. Wang, Enhanced Efficient Solar Evaporation of Co/CoO Loaded on the Tobacco Stem Under Visible Light, Advanced Sustainable Systems, 8 (2024) 2400349.

[71] Z. Shi, Y. Dong, Y. Chen, B. Wang, H. Wang, One-step synthesis of biocarbon based nano zero-valent iron for efficient Rhodamine B removal in Fenton-like reactions, Desalination and Water Treatment, 299 (2023) 190-202.

[72] M.Z.M. Nasir, M.A.A. Zaini, M.A.C. Yunus, Adsorption profiles of rhodamine B and reactive orange 16 onto pharmaceutical-based activated charcoals, Desalination and Water Treatment, 132 (2018) 340-349.

[73] S. Olivera, K. Venkatesh, M.S. Santosh, D. Leybo, D. Kuznetsov, B.K. Jayanna, A.M. Asiri, K.A. Alamry, H.B. Muralidhara, Open ended tube like hollow bio-carbon derived from banana fibre for removal of anionic and cationic dyes, Desalination and Water Treatment, 132 (2018) 297-306.

Open Access Article. Published on 20 November 2025. Downloaded on 12/25/2025 12:38:03 AM.
This article is licensed under a Creative Commons Attribution-NonCommercial 3.0 Unported Licence.

RSC Sustainability Accepted Manuscript

Data availability

View Article Online
DOI: 10.1039/D5SU00525F

Data sharing not applicable – no new data generated. Data availability is not applicable to this article as no new data were created or analysed in this study.

Open Access Article. Published on 20 November 2025. Downloaded on 12/25/2025 12:38:03 AM.
This article is licensed under a Creative Commons Attribution-NonCommercial 3.0 Unported Licence.

RSC Sustainability Accepted Manuscript